iScience

CellPress
OPEN ACCESS

Article

Single-cell transcriptome profiling reveals immune and stromal cell heterogeneity in primary Sjögren's syndrome

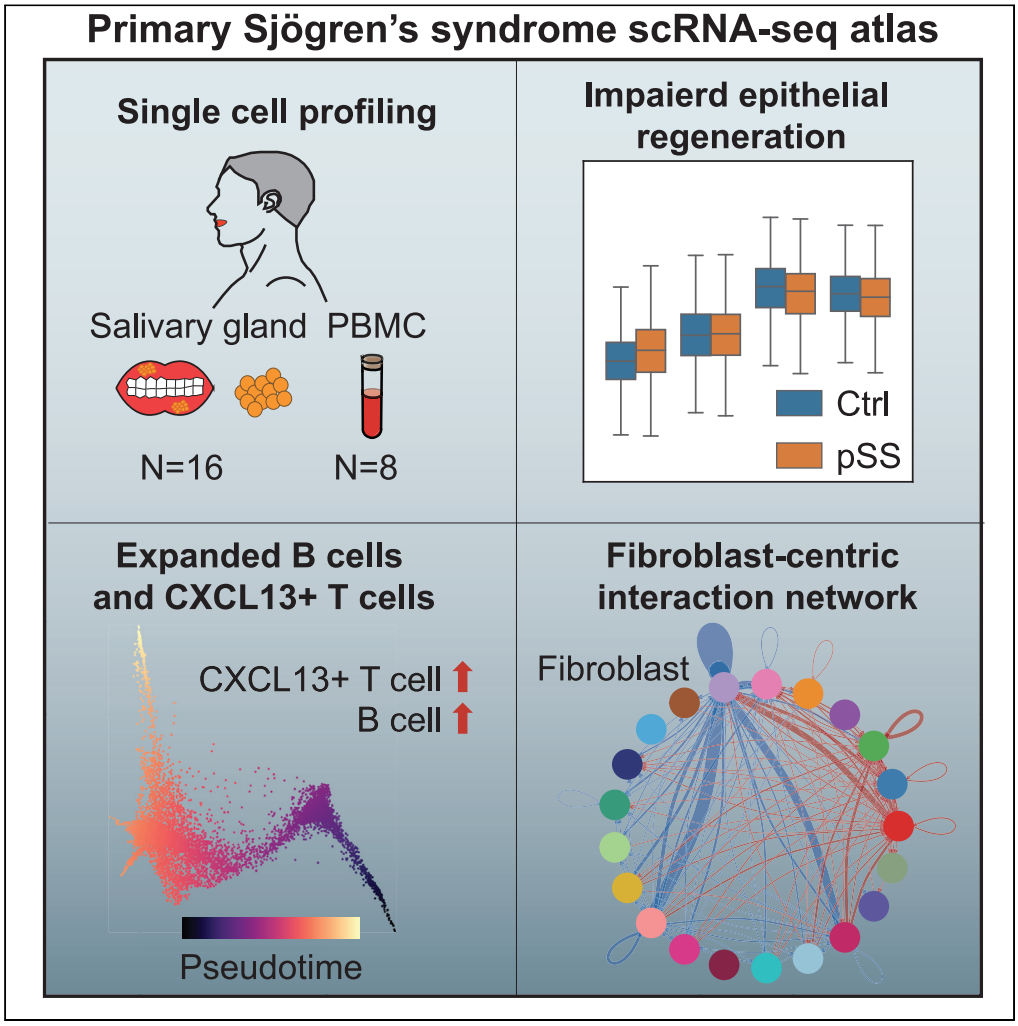

Nan Xiang, Hao Xu, Zhou Zhou, ..., Zhuo Chen, Chuang Guo, Xiaomei Li

gchuang@ustc.edu.cn (C.G.)
lixiaomei@ustc.edu.cn (X.L.)

Highlights

Elevated *ACKR1*$^{+}$ endothelial cells in pSS may promote transendothelial migration

SOX9 plays a vital role in epithelial cell regeneration and differentiation in pSS

Heterogeneity of B and CD4^{+} T cells in peripheral blood and salivary glands of pSS

Fibroblast subsets are pivotal for cell-cell interactions in pSS salivary glands

Xiang et al., iScience *26*, 107943
October 20, 2023
https://doi.org/10.1016/j.isci.2023.107943

iScience

CellPress
OPEN ACCESS

Article

Single-cell transcriptome profiling reveals immune and stromal cell heterogeneity in primary Sjögren's syndrome

Nan Xiang,[1,4] Hao Xu,[2,4] Zhou Zhou,[1] Junyu Wang,[2] Pengfei Cai,[2] Li Wang,[1] Zhen Tan,[1] Yingbo Zhou,[1] Tianping Zhang,[1] Jiayuan Zhou,[1] Ke Liu,[2] Songwen Luo,[2] Minghao Fang,[2] Guosheng Wang,[1] Zhuo Chen,[3] Chuang Guo,[1,2,*] and Xiaomei Li[1,5,*]

SUMMARY

Primary Sjögren's syndrome (pSS) is a complex autoimmune disease characterized by lymphocytic infiltration and exocrine dysfunction, particularly affecting the salivary gland (SG). We employed single-cell RNA sequencing to investigate cellular heterogeneity in 11 patients with pSS and 5 non-SS controls. Notably, patients with pSS exhibited downregulated SOX9 in myoepithelial cells, potentially associated with impaired epithelial regeneration. An expanded ACKR1$^+$ endothelial subpopulation in patients with pSS suggested a role in facilitating lymphocyte transendothelial migration. Our analysis of immune cells revealed expanded IGHD$^+$ naive B cells in peripheral blood from patients with pSS. Pseudotime trajectory analysis outlined a bifurcated differentiation pathway for peripheral B cells, enriching three subtypes (VPREB3$^+$ B, BANK1$^+$ B, CD83$^+$ B cells) within SGs in patients with pSS. Fibroblasts emerged as pivotal components in a stromal-immune interaction network, potentially driving extracellular matrix disruption, epithelial regeneration impairment, and inflammation. Our study illuminates immune and stromal cell heterogeneity in patients with pSS, offering insights into therapeutic strategies.

INTRODUCTION

Primary Sjögren's syndrome (pSS) is a complex, heterogeneous, systemic autoimmune disease that causes secretory gland dysfunction and can severely impact the quality of life.[1–3] Current treatment approaches for pSS are relatively effective for alleviating symptoms, and many clinical trials of immune targeting therapies in pSS have failed.[4] Patients with pSS exhibit focal lymphocytic sialadenitis in the salivary gland (SG), supporting the SG as the pathogenic center and primary damaged organ in pSS. CD4$^+$ T cell lymphopenia in the peripheral blood has been reported in patients with pSS, which may be explained by increased lymphocyte migration from the periphery to inflammatory sites.[5] Thus, a comprehensive understanding of cellular heterogeneity in the SG to define commonalities and discrepancies between the SG and peripheral blood immune cell populations can be informative of the mechanisms leading to pSS pathogenesis.

The stromal cells of the SG include the endothelium, epithelium, and fibroblasts.[6] Epithelial cells serve as the local source of autoantigens and participate in lymphoid cell survival, activation, and differentiation through the expression of multiple chemokines, inflammatory cytokines, and costimulatory molecules.[7–10] The SG epithelium includes several different cell types responsible for maintaining normal saliva secretion, including acinar, myoepithelial, and ductal cells. The pathogenesis of autoimmune epithelitis in patients with pSS is associated with aberrant expression of proteins involved in saliva secretion and the apoptosis of ductal and acinar cells, leading to secretory dysfunction.[11] The endothelial cells of patients with pSS express cell adhesion molecules, selectins, and chemokines at high levels.[12,13] These molecules reportedly promote lymphocyte transendothelial migration (TEM) during the inflammation process.[14] However, the molecular mechanism controlling TEM in the SG of patients with pSS is still unknown. Fibroblasts can produce soluble chemokines (e.g., CXCL13 and CCL19) involved in the recruitment of immune cells, and promote the survival of B and T cells.[15] A clear understanding of the cellular and molecular mechanisms underpinning secretory dysfunction and lymphocyte infiltration in the SG can guide the development of targeted therapeutics for pSS.

[1]Department of Rheumatology and Immunology, The First Affiliated Hospital of USTC, Division of Life Sciences and Medicine, University of Science and Technology of China, Hefei 230001, China
[2]Division of Molecular Medicine, Hefei National Laboratory for Physical Sciences at Microscale, School of Basic Medical Sciences, Division of Life Sciences and Medicine, University of Science and Technology of China, Hefei 230021, China
[3]Department of Pathology, The First Affiliated Hospital of USTC, Division of Life Sciences and Medicine, University of Science and Technology of China, Hefei 230001, China
[4]These authors contributed equally
[5]Lead contact
*Correspondence: gchuang@ustc.edu.cn (C.G.), lixiaomei@ustc.edu.cn (X.L.)
https://doi.org/10.1016/j.isci.2023.107943

In pSS, ductal cells of the SG are typically surrounded by infiltrating $CD4^+$ T cells and B cells that migrate from the periphery to the gland.[16] Decreased numbers of $CD4^+$ T cells have been reported in the blood of patients with pSS, implying a link between pSS and lymphopenia.[5] In the inflamed glandular tissues, $CD4^+$ effector subpopulations (e.g., Th1 cells, Th17 cells) contribute to pathogenesis by producing pro-inflammatory cytokines, thereby inducing B cell activation, and promoting the formation of an ectopic germinal center.[17] In comparison with healthy controls, patients with pSS have a smaller percentage of $CD27^+$ memory B cells in their peripheral blood and a greater proportion of $CD27^+$ memory B cells in the SG.[18] Furthermore, the overall percentages of activated B cells and long-lived autoantibody-producing plasma cells are higher in ectopic lymphoid structures of the SG.[19] These alterations in the immune microenvironment result in deep modifications to and impaired function of the glandular tissue in patients with pSS, therefore presenting several pressing questions that require the exploration of the interactions between infiltrated immune cells and other cells in the SG.

Here, we applied single-cell transcriptome sequencing (scRNA-seq) to profile 72,853 cells from the SG and 55,203 cells from peripheral blood mononuclear cell (PBMC) populations in a total of 16 patients with pSS and 8 non-SS controls. This analysis revealed significant downregulation of the epithelial cell regeneration-associated transcription factor, SOX9, in myoepithelial cells of patients with pSS. Furthermore, we identified an expanded $ACKR1^+$ endothelial subpopulation associated with enhanced lymphocyte transendothelial migration in patients with pSS. Examination of immune cell populations identified at least five B and $CD4^+$ T cell subpopulations that were specifically expanded in the SG of patients with pSS. Additionally, pseudotime trajectory analysis defined a bifurcated differentiation pathway for peripheral B cells and a trajectory leading to three distinct subtypes for peripheral $CD4^+$ T cells enriched in the SG of patients with pSS. Finally, an interaction network of the major cell types in the immune microenvironment in the disease state implicated SG fibroblasts in the disruption of extracellular matrix formation, impaired epithelial regeneration, and inflammation progression. The current study thus provides a comprehensive perspective of cellular heterogeneity in the SG and PBMCs of patients with pSS, subsequently enhancing our understanding of the pathogenic immune microenvironment in pSS to facilitate advances in therapeutic development.

RESULTS

Cell atlas of the salivary gland in patients with primary Sjögren's syndrome

We obtained 11 human salivary gland (SG) biopsy samples from patients with primary Sjögren's syndrome (pSS) and 5 SG samples from non-SS control individuals. For each SS patient, detailed clinical characteristics were recorded at the time samples were collected (summarized in Table S1). Using ESSDAI[20] to determine their disease activity index (DAI), all patients with pSS were established to present with apparent disease syndrome, showing an average of ESSDAI >6. The SG tissues were digested into single-cell suspensions and subjected to single-cell RNA sequencing (scRNA-seq) using the 10XGenomics Chromium platform (Figure 1A). After quality control (QC) processing (see STAR Methods), we obtained a total of 72,853 high-quality single-cell transcriptomes (Figures S1A–S1D). Of these, 49,097 cells originated from patients with pSS and 23,756 cells were from non-SS controls (Figure 1B). Seurat[21] was applied to normalize and cluster the gene expression data, subsequently generating a matrix that identified 11 unique, major cell subpopulations, which were visualized by uniform manifold approximation and projection (UMAP) (Figure 1B). The cell lineages of epithelial cells, ionocytes, fibroblasts, smooth muscle cells (SMC), endothelial cells, pericytes, melanocytes, T cells, B cells, plasma cells, and myeloid cells were identified based on the expression of known cell type-specific marker genes (Figures 1C and S2).

To delineate the differences in the SG landscape between pSS and non-SS controls, we first checked for divergence in the proportion of major cell types. While no apparent difference was observed between pSS and non-SS controls in the ratio of fibroblasts, endothelial cells, myeloid cells, and plasma cells, pSS samples had significantly greater T and B cell populations (Figure 1D). We noticed that epithelial cell populations also showed a noteworthy trend of lower abundance in the patients with pSS (Figure 1D). Furthermore, the proportions of several cell types (e.g., myeloid cells, mucous acinar, $CD4^+$T, and B cells) were correlated with the ESSDAI/anti-SSA, IgG, and ESR levels of patients with pSS, respectively (Figure S1E). Pairwise comparisons of the relative gene expression of predominant SG cell types between patients with pSS and non-SS controls identified 10,158 total differentially expressed genes (DEGs). In addition, epithelial cells of pSS samples had obviously higher numbers of DEGs than other cell types, including endothelial cells, fibroblasts, SMC, T cells, B and plasma cells, and myeloid cells (Figure 1E), indicating that epithelial cells underwent the most substantial transcriptomic changes of all cell types in the SG of patients with pSS.

Decreased SOX9 expression in myoepithelial cells impairs epithelial cell regeneration in patients with primary Sjögren's syndrome

Since epithelial cells are the major target of this disease,[22] we characterized their subpopulations and biological functions in the SG microenvironment of patients with pSS and non-SS controls. In total, 27,742 epithelial cells were detected, among which four previously described subpopulations emerged, including serous acinar cells, mucous acinar cells, ductal cells, and myoepithelial cells, based on their expression of canonical markers (Figures 2A, 2B, S3A, and S3B). No significant differences were observed in the proportions of epithelial cell subpopulations between patients with pSS and non-SS controls ($p > 0.05$, Figure S3C). Comparison of transcriptomic divergence for each epithelial subpopulation between patients with pSS and non-SS controls revealed enrichment for interferon signaling (e.g., *IFI27*, *IFI44L*, *IFITM1*, *IFI6*) and MHC-II pathway (e.g., *HLA-DQA1*, *HLA-DQB1*, *HLA-DRA*) in the upregulated DEGs of pSS epithelial cells (Figure 2C), and moreover, these signaling pathways were significantly upregulated in all four epithelial cell subpopulations (Figure 2D). Notably, we identified several clinical features (e.g., IgM and IgG) that could potentially affect the expression of genes related to these functions (Figure S3D). These results

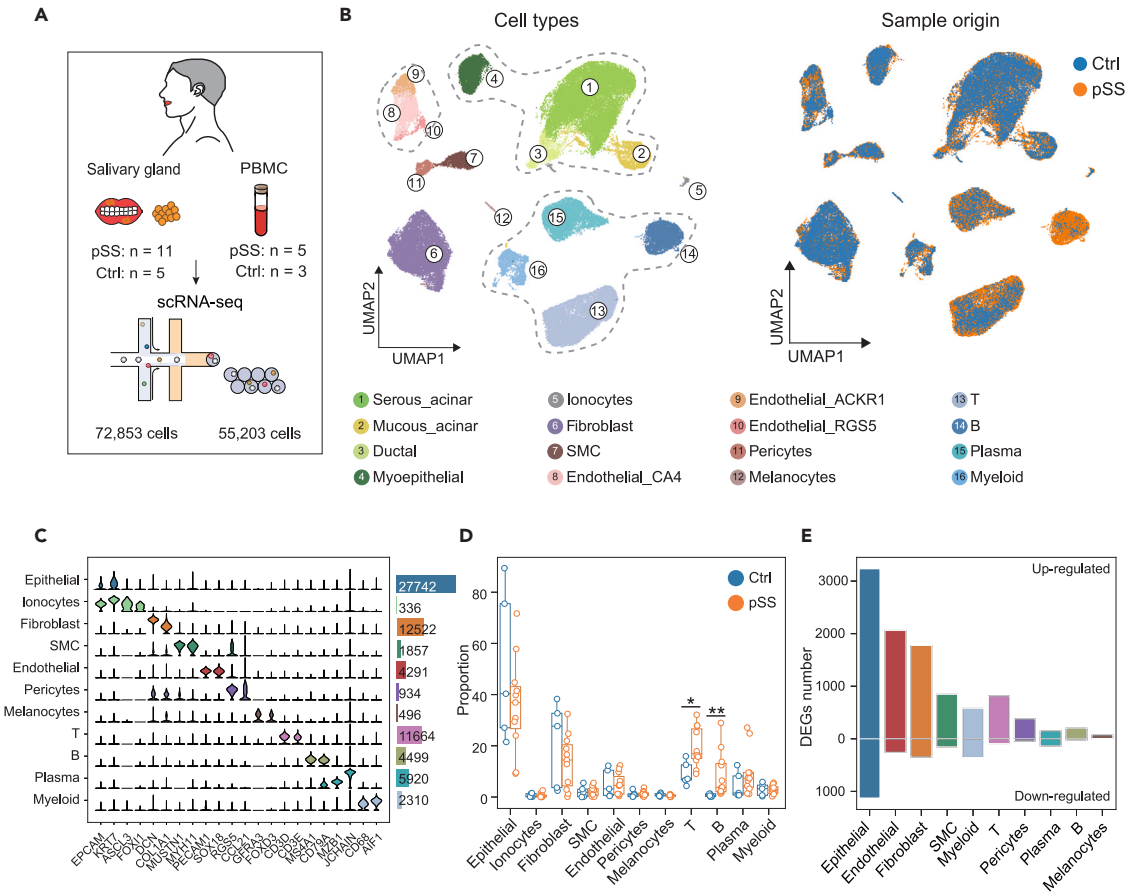

Figure 1. Single-cell RNA-seq of the salivary gland from pSS patients and non-SS controls

(A) Flowchart depicting the overall design of the study. Summary of the number of samples collected and single-cell RNA sequencing data produced by this study. n, number of subjects.

(B) UMAP plot showing the distribution of cells in SG colored by cell subset annotation (left) and sample origin (right).

(C) Violin plots showing the expression of selected marker genes in each cell type. Bar plot on the right showing the cell numbers in each cell subset.

(D) Boxplots of the cell proportions of cell subsets by comparing pSS patients with non-SS controls in the SG. *$p < 0.05$, **$p < 0.01$, Wilcoxon rank-sum test. Center line, median value; box limits, upper and lower quartiles; whiskers, 1.5× interquartile range.

(E) Bar plots of the differentially expressed genes (DEGs) in each cell subset.

suggested a possible coordinated transcriptomic program in SG epithelial cell subpopulations of patients with pSS, characterized by aberrant interferon signaling and antigen presentation (Figure S3E).

Gene ontology (GO) analysis of down-regulated DEGs, which similarly point to global transcriptional shifts in SG epithelial cells of patients with pSS, indicated that functional annotations related to "salivary secretion," "regulation of cell cycle process," and "epithelial cell differentiation" were enriched in these DEGs (Figure S3F). Assessment of the expression levels for these GO term-associated genes showed that they were significantly reduced in all four epithelial cell subpopulations, especially ductal cells and myoepithelial cells (Figure 2E). For example, the salivary mucin component gene, *MUC7*, was decreased in ductal and myoepithelial cells of patients with pSS (Figure 2C). *ZG16B*, co-expressed with MUC7 and enriched in healthy human SG acinar cells,[23] was significantly decreased in ductal and myoepithelial cells of patients with pSS. In addition, expression of *AQP5*, a water transporter in saliva fluid secretion,[24] was decreased in ductal cells of patients with pSS. *PIP*, which reportedly controls AQP5 localization in the human SG,[25] was decreased in ductal cells of patients with pSS (Figure 2C). These data also showed that the epithelial differentiation regulator, *DMBT1*, was significantly downregulated in ductal cells of patients with pSS (Figure 2C). These collective results aligned well with impaired salivary secretion, regeneration, and differentiation function in SG epithelial cells of Sjögren's syndrome.

To explore transcription factors (TFs) potentially responsible for the aberrant regulation of disease-associated transcriptional programs in epithelial cells, we used SCENIC[26] to predict TFs involved in the downregulation of epithelial cell subpopulations of patients with pSS. In particular, *SOX9*, which has been reported as an essential regulator in SG development,[27] emerged as the TF most significantly associated with "epithelial cell differentiation" (Figure 2F). To further validate the role of SOX9, we explored publicly available RNA-seq data[28] from a breast cancer epithelial cell line with SOX9 knockdown to identify the suite of genes affected by its loss of activity. We then examined the

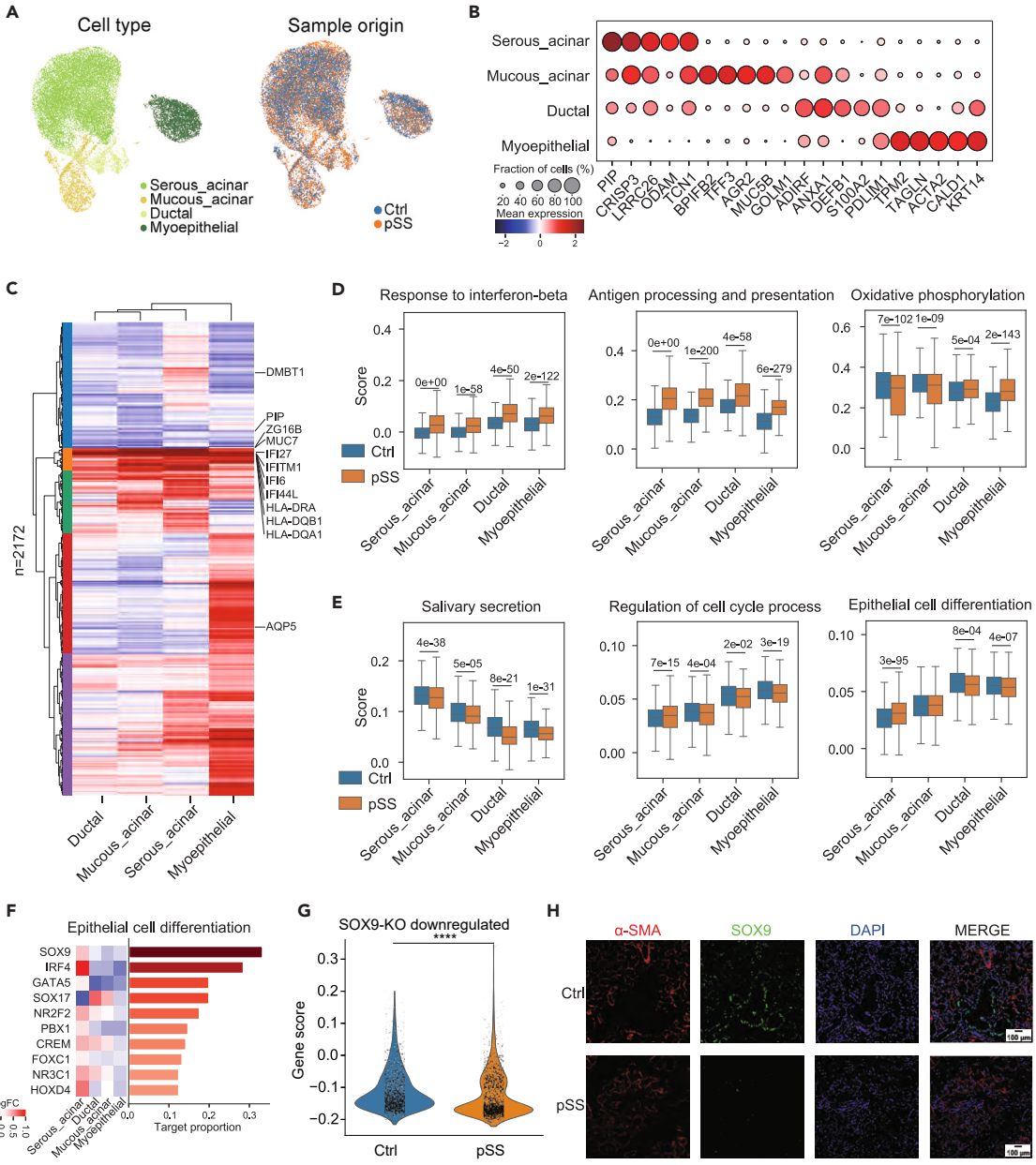

Figure 2. Epithelial cell regeneration dysfunction in pSS patients

(A) UMAP plot showing the distribution of epithelial cells in SG colored by cell subset (left) and sample origin (right).

(B) Dot plots showing the top 5 genes of each cell subset of epithelial cells. Each dot is colored by the mean expression and sized by the fraction of expressed cells.

(C) Heatmap showing the differentially expressed genes (DEGs) in each cell subset of epithelial cells between pSS patients and non-SS controls.

(D and E) Boxplots showing the up-regulated (D) and down-regulated (E) gene set scores of each cell subset compared between non-SS controls and pSS patients. Center line, median value; box limits, upper and lower quartiles; whiskers, 1.5× interquartile range. *p* values are shown above the box, Wilcoxon rank-sum test.

(F) Bar plots of the proportion of target genes in the epithelial cell differential gene set regulated by TFs predicted from SCENIC.

(G) SOX9 knockout gene set score in the pSS patients and non-SS controls. ****p < 0.0001, Wilcoxon rank-sum test.

(H) Immunofluorescence of alpha-SMA (red), SOX9 (green), and DAPI (blue) in pSS patients (n = 5) and non-SS controls (n = 5) in SG. Scale bar, 100 μm.

expression of these SOX9 targets in our current scRNA-seq and found that they were also significantly downregulated in patients with pSS (Figures 2G and S3H). Functional annotations of the SOX9 target genes showed enrichment related to "epithelial cell differentiation" (Figure S3G), indicating that the downregulation of SOX9 may contribute to the dysregulation of epithelial cell differentiation in patients with

pSS. Immunofluorescence staining assays to characterize the spatial co-localization of SOX9 with myoepithelial cells revealed that SOX9 aggregated with myoepithelial cells in non-SS SG tissues, but its expression was significantly reduced, almost undetectable under disease conditions (Figure 2H). These findings of decreased SOX9 and its target gene expression, combined with the strikingly decreased SOX9 immunofluorescence signal in myoepithelial cells, suggest that SOX9 contributes to the transcriptional regulation of myoepithelial cell regeneration and that the loss of SOX9 expression may lead to impaired epithelial cell regeneration and differentiation in patients with pSS.

ACKR1$^+$ endothelial cells could enhance lymphocyte transendothelial migration in patients with primary Sjögren's syndrome

Since endothelial cells function as the barrier between blood and tissues which controls lymphocyte activation, adhesion, and transmigration,[29] we explored the features and functions of endothelial subpopulations in patients with pSS and non-SS controls. Using further clustering analysis, we identified three distinct endothelial subpopulations, including CA4$^+$ endothelial cells, previously identified as capillary endothelial cells,[30] ACKR1$^+$ endothelial cells, which displayed the gene signature of venous endothelial cells,[31] and RGS5$^+$ endothelial cells, comprised of cells undergoing endothelial–mesenchymal transition (EndoMT)[32] (Figures 3A and S4A–S4C). Although the comparison of total endothelial populations showed no significant differences in the endothelial proportion between patients with pSS and non-SS controls (Figure 1D), the comparison of endothelial subpopulations revealed that the proportion of ACKR1$^+$ cells was significantly higher ($p = 0.011$) in the SG of patients with pSS (Figure 3B). Identification of DEGs in the three endothelial cell subpopulations between patients with pSS and non-SS controls showed that ACKR1$^+$ endothelial cells had a larger number of DEGs than the other two subtypes (Figure 3C), suggesting that this cell subpopulation was predominantly responsible for the observed changes in endothelial cells between patients with pSS and non-SS controls.

Phenotypically, compared to non-SS controls, ACKR1$^+$ endothelial cells of patients with pSS exhibited higher expression of chemokine-related genes (e.g., *CXCL11*, *CXCL10*, *CXCL2*), *VCAM1*, and *SELE*, which reportedly mediate the lymphocyte transendothelial migration (TEM) process[33] (Figures 3D and S4D). GO analysis indicated that pSS ACKR1$^+$ endothelial cells were enriched with DEGs related to the "regulation of leukocyte migration" (Figures 3E and S4E). To verify that ACKR1$^+$ endothelial cells were enriched in the SG of patients with pSS, we conducted immunofluorescence detection of ACKR1 expression in the SG of patients with pSS and non-SS controls. These experiments confirmed that ACKR1 expression was higher in endothelial cells of patients with pSS than in non-SS controls (Figure 3F).

To investigate the specific trajectories of the three endothelial subpopulations throughout the course of endothelial cell differentiation in the SG, we used Palantir[34] to construct a model of the differentiation potential trajectory for all endothelial cells collected from patients with pSS and non-SS controls. Two developmental branches clearly emerged where CA4$^+$ endothelial cells differentiated into ACKR1$^+$ endothelial cells or into RGS5$^+$ endothelial cells (Figures 3G and 3H). Moreover, this pseudo-time trajectory showed that the proportion of cells differentiating into ACKR1$^+$ endothelial cells was greater in patients with pSS than that in non-SS controls, ultimately comprising 44.0% vs. 33.2%, respectively, of the total endothelial population (Figure 3I). This finding was consistent with the above results showing enrichment for the "regulation of leukocyte migration" in ACKR1$^+$ endothelial cells of patients with pSS (Figure S4F). In summary, these findings suggested that the ACKR1$^+$ endothelial cell subpopulation could promote lymphocyte TEM from circulation to the SG in patients with pSS.

B cells originating in peripheral blood differentiate and expand in the salivary gland of patients with primary Sjögren's syndrome

Local immune cells in the SG, especially infiltrated CD4$^+$ T and B cells, have been firmly linked to migration from the peripheral circulating blood.[35] To investigate the relative heterogeneity of immune cells in peripheral blood and SG tissue of patients with pSS, we performed a separate scRNA-seq experiment using peripheral blood mononuclear cells (PBMCs) isolated from 5 patients with pSS and 3 healthy controls in an independent cohort (Figures 1A and S5A; Table S2). Using a reciprocal principal component analysis method[36] for the integration of PBMCs and SG scRNA-seq data, we obtained a total of 79,596 immune cell transcriptomes. Among these, we identified five major populations and 36 immune cell clusters, including 4 B cell clusters, 4 plasma cell clusters, 19 T cell clusters, 8 myeloid cell clusters, and natural killer (NK) cells (Figures 4A and 4B). No obvious differences were found in the ratio of myeloid cells, plasma cells, or NK cell clusters in PBMCs and SG between patients with pSS and non-SS controls, although significant alterations were detected in the proportions of CD4$^+$ T or B cell clusters (Figures S5B and S5C). To further validate the proportion alterations of CD4$^+$ T or B cell clusters in PBMCs, we mapped previously reported scRNA-seq data of PBMCs from patients with pSS and non-SS controls[37] to our scRNA-seq data for cell cluster annotation. We again observed significant enrichment of CD4$^+$ T and B cell clusters in PBMCs from patients with pSS compared with those from non-SS controls (Figure S5D).

Closer examination of these cell clusters indicated that the proportions of VPREB3$^+$ memory B, BANK1$^+$ effector memory B, and IGHD$^+$ naive B cell clusters were higher in the SG of patients with pSS than that in the SG of non-SS subjects (Figures S5B and S6A). CD83$^+$ effector B cell showed a trend of higher abundance in SG of patients with pSS (Figures S5B and S6A). We also noted that IGHD$^+$ naive B cell cluster was expanded in the PBMCs of patients with pSS compared with that in non-SS controls (Figure S5C). A subsequent flow cytometry analysis on B cell subsets also showed that the number of IGHD$^+$ B cell cluster was significantly increased in patients with pSS compared to healthy controls ($p < 0.05$, Figure S7). Enrichment analysis of overall cell proportions indicated that all B cell clusters showed greater enrichment in the SG than in the periphery of patients with pSS (Figure 4C). Furthermore, undirected graph analysis of the major cell clusters showed that B cell clusters displayed the highest degree of transcriptomic divergence between pSS and non-SS subjects, as well as between SG and PBMC samples (Figure S6B). The local expansion of B cells in SG supported the likelihood that this subpopulation follows a specific trajectory of differentiation and activation in patients with pSS.

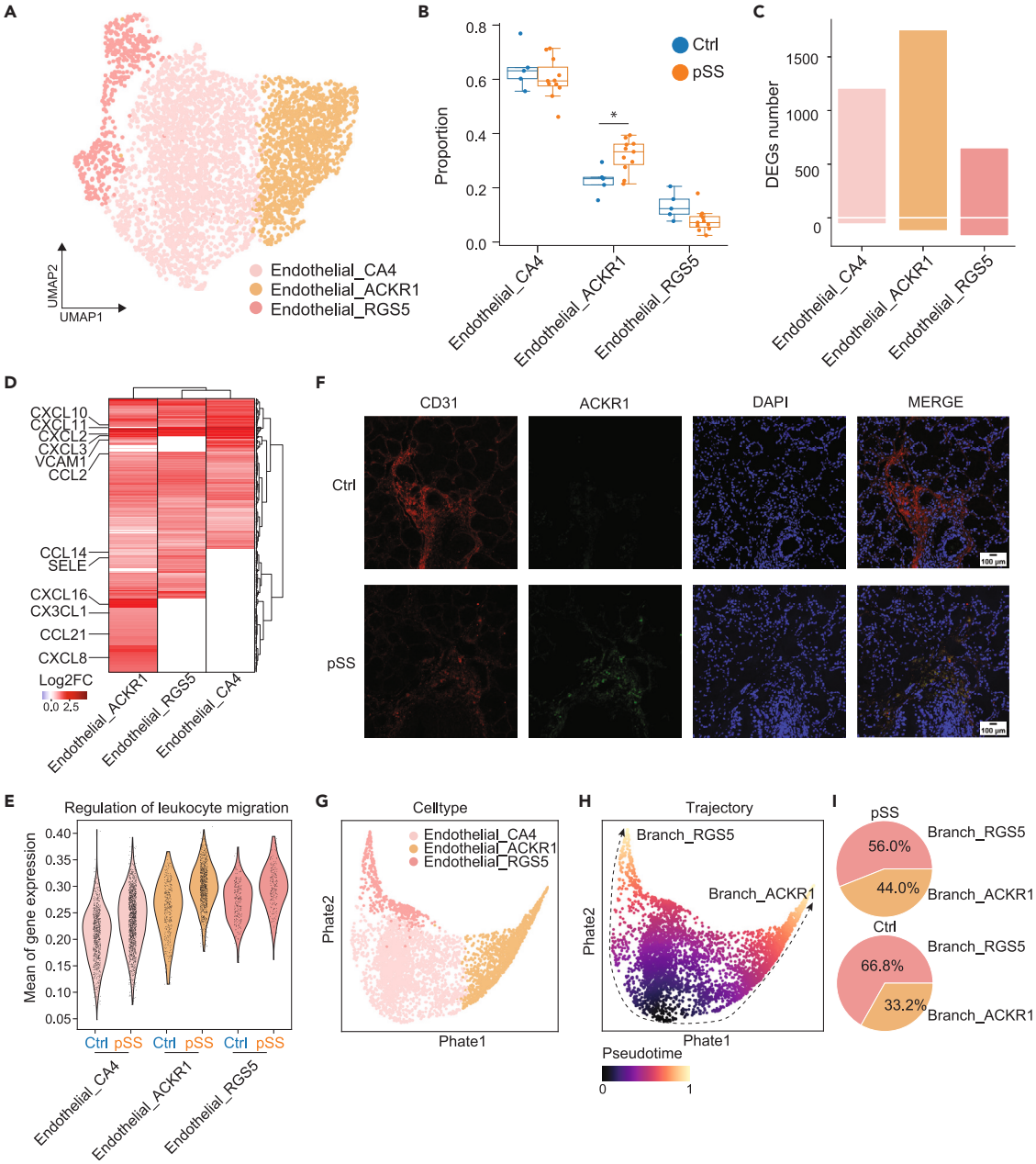

Figure 3. Phenotypic and functional characterization of endothelial cells in salivary gland

(A) UMAP plot showing the distribution of endothelial cells in SG colored by cell subset.

(B) Boxplots of the cell proportions of endothelial cell subsets in pSS patients and non-SS controls in the SG. Center line, median value; box limits, upper and lower quartiles; whiskers, 1.5× interquartile range. *p < 0.05, Wilcoxon rank-sum test.

(C) Bar plots of the DEGs numbers in each cell subset of endothelial cells.

(D) Heatmap showing the DEGs in each cell subset of endothelial cells between pSS patients and non-SS controls.

(E) Violin plots showing the average gene expression of the term 'regulation of leukocyte migration'.

(F) Immunofluorescence of CD31 (red), ACKR1 (green) and DAPI (blue) in pSS patients (n = 5) and non-SS controls (n = 5) in SG. Scale bar, 100 μm.

(G) Scatterplots showing the distribution of endothelial cells in SG embedded in PHATE.

(H) Scatterplots showing the pseudotime of each endothelial cell with PHATE embedding.

(I) Pie plots of the cell proportion of each branch of the trajectory in pSS patients and non-SS controls in the SG.

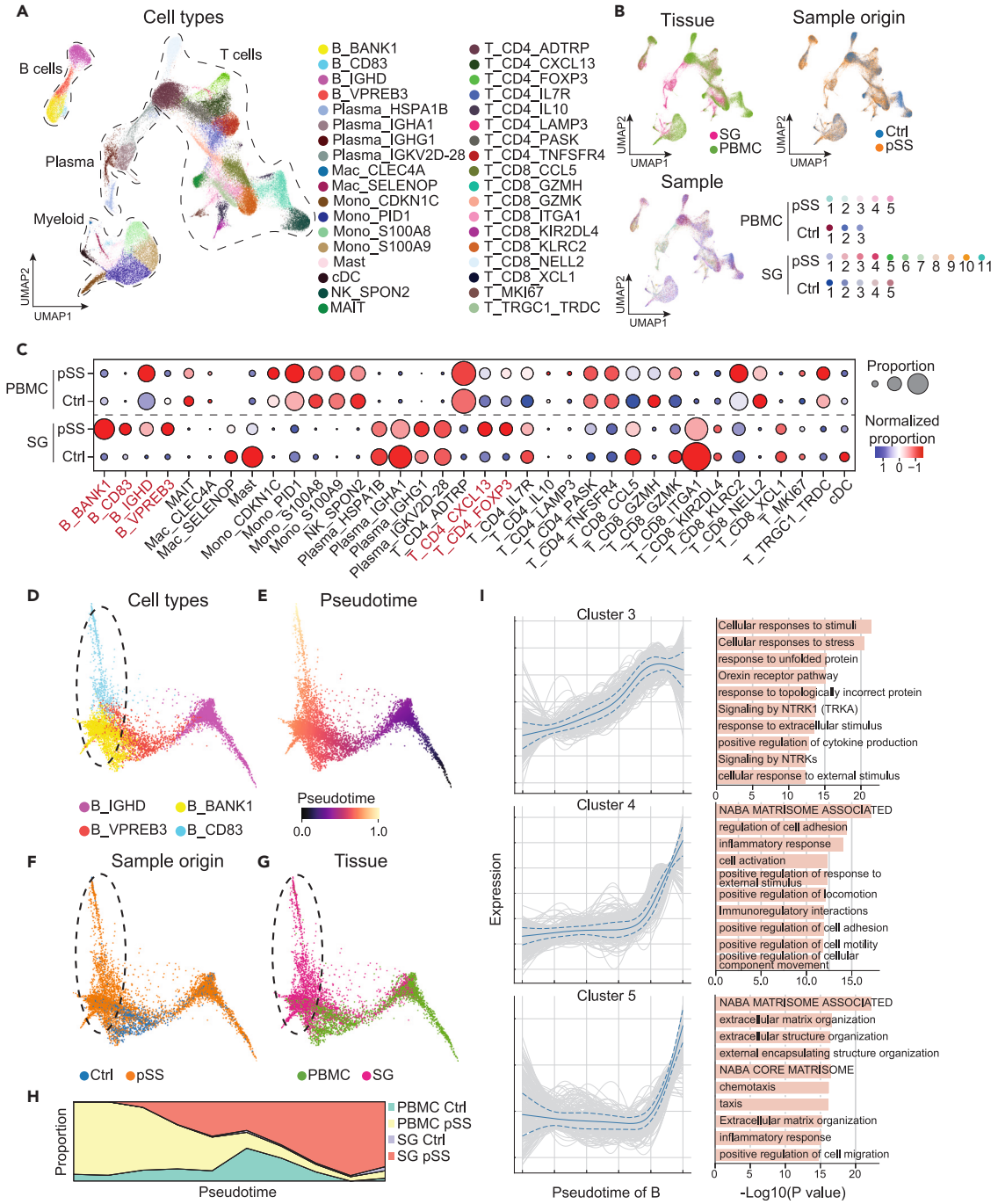

Figure 4. B cells expand in the SG of pSS patients with a trajectory differentiate from peripheral blood

(A) UMAP plot showing the distribution of immune cells in SG and PBMCs colored by cell subsets.

(B) UMAP plot showing the distribution of immune cells in SG and PBMCs colored by tissue, sample origin and sample.

(C) Dot plots showing the cell proportion of each cell subset comparison in each tissue and each sample origin. Each dot is colored by normalized proportion that z-scored by column and sized by the proportion.

(D) Scatterplot of B cells distribution colored by cell subsets in PHATE embedding.

(E) Scatterplot of B cells distribution colored by pseudotime in PHATE embedding.

(F) Scatterplot of B cells distribution colored by sample origin in PHATE embedding.

(G) Scatterplot of B cells distribution colored by tissues in PHATE embedding.

(H) Line plot showing the cell proportion differences in each tissue and each sample origin along with pseudotime.

(I) Line plot showing the expression pattern of gene clusters 3, 4, and 5 along with the pseudotime of B cells. Bar plots showing the top 5 gene terms enriched in gene clusters 3, 4, and 5.

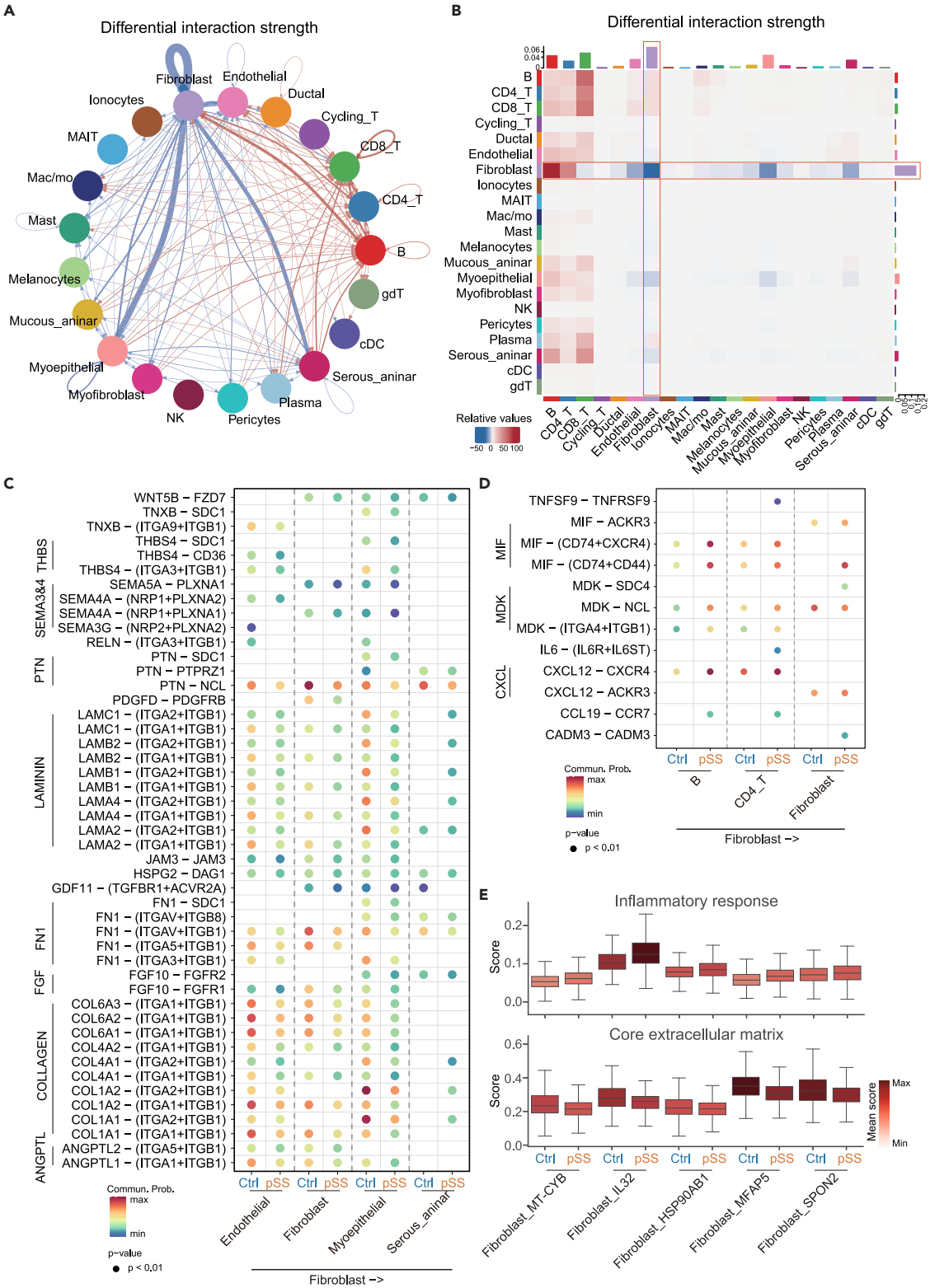

Figure 5. Cell-cell interaction network in pSS patients

(A) Circle plot showing the differential interaction strength in the cell-cell communication network, where red (or blue) colored edges represent increased (or decreased) signaling in pSS patients compared to non-SS controls.

Figure 5. *Continued*

(B) Heatmap showing the differential interaction strength of the cell-cell communication network. The colored bar plot in the top represents the sum of the column of values displayed in the heatmap (targets signaling/receptors). The right colored bar plot represents the sum of the row of values (sources signaling/ligands). In the color bar, red (or blue) represents increased (or decreased) signaling in the pSS patients compared to the non-SS controls.

(C and D) Dot plots of predicted receptor/ligand interactions of fibroblasts with non-immune cell subsets (endothelial, myoepithelial and serous acinar cells) (C) and immune cells (B and $CD4^+$ T cells) (D) in the pSS patients and the non-SS controls. The expression levels of all the interacting genes were scaled by color. *p* values are shown by circle size ($p < 0.01$), Wilcoxon rank-sum test.

(E) Boxplots showing the gene expression score of up-regulated and down-regulated ligands for each cell subset in fibroblasts. Center line, median value; box limits, upper and lower quartiles; whiskers, 1.5× interquartile range.

To delineate the hierarchy and developmental relationship between B cell subpopulations, we applied Palantir[34] to determine the order of each pSS or non-SS single-cell transcriptome in the pseudotime trajectory. This analysis showed that the progression proceeded from $IGHD^+$ B to $VPREB3^+$ B and $BANK1^+$ B, and then to $CD83^+$ B (Figures 4D and 4E). We also identified the differentiation pathway wherein B cells exhibit an apparent tendency to migrate from peripheral blood to the SG (Figures 4F and 4G), with a higher proportion of B cells in the SG of patients with pSS at the end of pseudotime (Figure 4H). To test this possibility, we then investigate trends in gene expression along pseudotime. This analysis defined three (clusters 3, 4, and 5) profiles comprised of gene clusters that were significantly upregulated along pseudotime (Figures 4I and S6C). GO analysis indicated that cluster 3 was enriched with genes involved in "cellular response to stimuli" and "response to extracellular stimulus" (Figure 4I). By contrast, genes in clusters 4 and 5 were upregulated at the end of pseudotime, and were enriched for terms such as "inflammatory response," "cell activation," "chemotaxis," and "positive regulation of cell migration" (Figures 4I and S6D). Notably, cluster 2 upregulated at the start of pseudotime while downregulated at the end of pseudotime and was enriched with genes involved in the "regulation of lymphocyte activation" and "regulation of leukocyte activation" (Figure S6D), suggesting that B cells are activated in peripheral blood but not SG. Moreover, DEG analysis in each B cell subpopulation between patients with pSS and non-SS controls, in both SG tissue and PBMCs, revealed that the large majority of DEGs between disease and non-disease samples were expressed in PBMC B cells, whereas SG B cells had considerably fewer DEGs (Figure S6E). GO analysis indicated that DEGs of peripheral blood B cells in patients with pSS enriched with genes involved in "cytokine signaling in immune system" and "regulation of leukocyte activation" (Figure S6F). These findings thus defined a differentiation pathway in which B cells are activated in peripheral blood, and then differentiated and expanded in the SG in pSS.

$CXCL13^+CD4^+$ T cells and $FOXP3^+$ Treg cells are enriched in the salivary gland of patients with primary Sjögren's syndrome

In light of the significant alterations detected in the proportions of $CD4^+$ T cells between patients with pSS and non-SS controls (Figures S5B and S5C), together with previous reports showing that this cell type infiltrates the SG in the early stage of pSS,[17] we therefore investigated the transcriptomic characteristics of peripheral and SG-associated $CD4^+$ T cells in patients with pSS. Subtyping identified eight total $CD4^+$ T subpopulations in the combined PBMCs and SG scRNA-seq (Figure 4A). Among them, no significant differences were found in the proportions of $CD4^+$ T cell subpopulations in pSS PBMCs compared with non-SS controls (Figure S5C). However, $ADTRP^+CD4^+$ naive $CD4^+$ T cells (expressing *MAL* and *LEF1*), $CXCL13^+CD4^+$ peripheral helper (Tph) T cells (expressing *CXCL13*, *ICOS,* and *PDCD1*), and $FOXP3^+CD4^+$ regulatory T (Treg) cells (expressing *FOXP3, LAYN,* and *RTKN2*) were significantly expanded in the SG of patients with pSS (Figures 4C and S5B). The flow cytometry results revealed a substantial increase in the proportion of $FOXP3^+CD4^+$ T cells, coupled with a reduction in the proportion of $IL10^+CD4^+$ T cells in PBMCs, among patients with pSS compared to healthy controls ($p < 0.05$, Figure S8). We then explored the developmental trajectory between $CD4^+$ T cell subpopulations. Construction of a pseudotime trajectory for $CD4^+$ T cells revealed three distinct branches leading to different $CD4^+$ T cell clusters aligned along pseudotime, starting with $ADTRP^+CD4^+$ T cells and ending with the $FOXP3^{hi}$, $CXCL13^{hi}$, and $TNFSFR4^{hi}CD4^+$ T cell clusters (Figure S9A). We also detected a greater number of $CXCL13^+CD4^+$ T and $FOXP3^+CD4^+$ T cells in the SG of patients with pSS at the end of pseudotime (Figure S9A). Several transcriptional profiles emerged in which different gene clusters enriched for the "regulation of lymphocyte activation," "regulation of T cell activation," and "regulation of cell activation" were significantly upregulated at various points in pseudotime (Figures S9B and S9C). Additionally, *CLTA-4, FOXP3*, T cell co-signal molecules (e.g., *TNFSF9* and *TNFSF14*), and MHC-II molecules (e.g., *HLA-DRB1* and *HLA-DQA1*) were also upregulated along pseudotime (Figure S9D). Our findings reveal an increased proportion of $CXCL13^+CD4^+$ T cells and $FOXP3^+$ $CD4^+$ Treg cells within the salivary gland of patients with pSS, shedding light on the differentiation pathway of $CD4^+$ T cells.

A fibroblast-centric ligand/receptor interaction network in patients with primary Sjögren's syndrome

To identify the dysregulated signaling pathways in the SG immune microenvironment of patients with pSS, we applied CellChat[38] to detect aberrant changes in the molecular interactions between various immune cell subpopulations and stromal cells, as well as within stromal cell populations (see STAR Methods). In particular, fibroblasts were found to form a dense communication network with other cells, including myoepithelial, endothelial, serous acinar, $CD4^+$ T, and B cells (Figures 5A and 5B). Moreover, the differential interaction strength of receptor and ligand signaling of fibroblasts (fibroblasts represent as targets and sources, respectively) was significantly downregulated in patients with pSS compared with that in non-SS controls (Figure S10A). These striking changes in the interactions between fibroblasts and other cell types in patients with pSS suggested that fibroblasts might play a central regulatory role in pSS progression.

We further investigated the specific fibroblast interactions that were altered in patients with pSS and found that the most significantly downregulated signaling pathways were the COLLAGEN, LAMININ, and FN1 pathways (Figures S10B and S10C). Specifically, fibroblasts

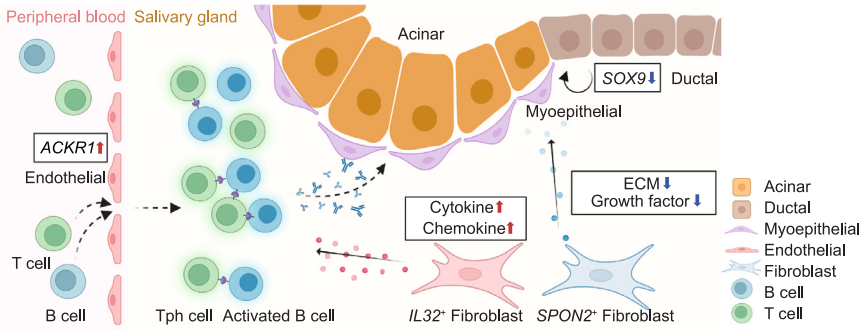

Figure 6. Multiple pathway alteration of fibroblast-centric in pSS

Within SG, SPON2$^+$ fibroblast downregulating growth signaling factors and extracellular matrix (ECM) components potentially contribute to the impairment of epithelial cell regeneration with SOX9 downregulation; IL32$^+$ fibroblast upregulating cytokines and chemokines could promote local inflammation by recruiting activated T cells and B cells. Within peripheral blood, T cells and B cells *trans*-endothelial migration through expanded ACKR1$^+$ endothelial cells.

showed decreased expression of ligand-receptor pairs that could contribute to the extracellular matrix organization, such as COL1A1-(ITGA1/ITGB1), LAMA2-(ITGA1/ITGB1), and FN1-(ITGAV/ITGB1) by interacting with myoepithelial, endothelial and serous acinar cells (Figure 5C). In addition, the expression of several growth factors signaling pathways (e.g., PDGF, TGFb, EGF, and FGF) which participate in SG development was decreased in the fibroblasts of patients with pSS (Figures S10B and S10C). Moreover, the strength of interactions between fibroblasts and myoepithelial, endothelial, or serous acinar cells involving Wnt signaling (e.g., WNT5B-FZD7) was also significantly lower in patients with pSS (Figure 5C). These results suggested that fibroblasts could potentially contribute to the impairment of epithelial cell regeneration and gland development in pSS.

Fibroblasts can assume different roles as inflammatory cells in autoimmune diseases.[39] Here, we detected several pro-inflammatory signaling pathways that were upregulated in fibroblasts of patients with pSS compared to the non-SS controls, including CXCL,[40] MIF,[41] and MK[42] (Figures S10B and S10C). These pSS-associated fibroblasts showed increased expression of chemokine ligand-receptor pairs interacting with CD4$^+$ T and B cells (e.g., CXCL12-CXCR4 and CCL19-CCR7), which could potentially enhance lymphocyte recruitment (Figure 5D). The strength of MIF ligand-receptor interactions (e.g., MIF-(CD74/CXCR4), MIF-(CD74/CD44)) and MK ligand-receptor interactions (e.g., MDK-NCL, MDK-(ITGA4/ITGB1)) between fibroblasts and CD4$^+$ T or B cells was also significantly increased in patients with pSS (Figure 5D), suggesting that fibroblasts could promote local inflammation through interactions with infiltrating immune cells in patients with pSS.

Further clustering analysis identified five distinct fibroblast subpopulations, including HSP90AB1$^+$, SPON2$^+$, MT-CYB$^+$, MFAP5$^+$, and IL32$^+$ fibroblasts (Figures S11A and S11B). Although no significant differences were observed in the proportions of fibroblast subpopulations between pSS and non-SS samples ($p > 0.05$, Figure S11C), IL32$^+$ fibroblasts in patients with pSS expressed high levels of pro-inflammatory molecules (e.g., *CXCL19*, *MIF*, *IL-6*, and *MDK*) (Figures 5E and S11D). This finding indicated that the IL32$^+$ fibroblast subpopulation was predominantly responsible for interactions with immune cells leading to local inflammation in patients with pSS. Additionally, collagen-related gene expression (e.g., *COL1A1*, *COL1A2*, and *COL6A1*) was lower in SPON2$^+$ fibroblasts of patients with pSS, suggesting that this cell subpopulation may contribute to disrupting extracellular matrix formation and epithelial regeneration (Figures 5E and S11E). Collectively, these findings illustrated the intercellular interactions among fibroblast, epithelial, endothelial, and immune cells in the SG that potentially lead to inflammatory and regeneration-impaired pSS phenotype (Figure 6), increasing the scope of our understanding of the local immune microenvironment in patients with pSS.

DISCUSSION

Previous studies have illustrated the distinct involvement of both immune cells and stromal cells in the pathogenesis of primary Sjögren's syndrome (pSS).[43] Although previous scRNA-seq analysis of PBMCs in patients with pSS has identified changes in several immune cell subsets,[37,44] an atlas-level integrative analysis of the salivary gland (SG) and peripheral blood is required for a comprehensive perspective of pSS development and progression. Here, we defined cell populations in the pSS immune microenvironment through single-cell transcriptome sequencing of the SG and PBMCs in two independent cohorts of patients with pSS and non-SS controls. This analysis identified a disease-associated epithelial subpopulation, myoepithelial cell, with characteristically low expression of SOX9, which leads to impaired regeneration of epithelial cells. We also found that patients with pSS have a strikingly increased number of ACKR1$^+$ endothelial cells that could potentially promote transendothelial migration from peripheral blood monocyte populations. Integrative analysis of local and peripheral immune cell transcriptomes identified the specific B cells and CD4$^+$T subpopulations which expanded in SG and PBMCs from patients with pSS respectively. Finally, we provide a series of detailed maps of the global interactions between immune cells and stromal cells, and among stromal cells. These interaction networks can guide future hypothesis-driven research of ligand/receptor interactions that may drive inflammatory response and glandular destruction in pSS.

Myoepithelial cells are known to function in gland tissue contraction, but their role in pSS is not well understood. Ninche and co-workers showed that myoepithelial cells exhibit remarkable cellular plasticity, which enables acinar regeneration after severe SG injury.[45] Myoepithelial cells can also function as reserve stem cells to regenerate airway epithelium after injury, with elevated SOX9 expression necessary for their phenotypic plasticity.[46] Moreover, SOX9 was previously shown to regulate stem cell properties in the SG and play an essential regulatory role in SG development and regeneration.[27,47] In this study, we validated the role of SOX9 by exploring the publicly available RNA-seq data from a breast cancer epithelial cell line with SOX9 knockdown. Previous cross-tissue studies using single-cell gene expression data provided evidence that various epithelial cells exhibit common features including both salivary and mammary glands.[48] SOX9 is also a key regulator in mammary gland development and stem/progenitor cell maintenance, as well as breast cancer stem cells.[49,50] Therefore, the numerous similarities shared between breast cancer epithelial cells and SG epithelial cells provide a solid rationale for our analysis. The above clues in combination with our own findings led us to hypothesize that the downregulation of SOX9 affects the stem-like properties of myoepithelial cells, ultimately leading to the defects in epithelial cell regeneration characteristic of pSS. To date, few studies have examined the regenerative function of myoepithelial cells or the regulatory contribution of SOX9 to pSS, leading to a gap in understanding of pSS pathogenesis.

Trans-endothelial migration (TEM) is a vital physiological process, but can lead to inflammatory disorders when it occurs in excess or at inappropriate locations.[14] Here, our findings suggest a potential role of ACKR1$^+$ endothelial cells in facilitating lymphocyte transendothelial migration in pSS. This population expresses high levels of *SELE* and *VCAM1*, encoding E-selectin and adhesion molecules, respectively, which contribute to rolling, arrest, and firm adhesion functions in circulating immune cells.[51,52] In addition, high expression of multiple chemokines by ACKR1$^+$ endothelial cells may trigger the expression of high-affinity LFA-1 integrin in lymphocytes, promoting lymphocyte crawling and probing for TEM sites.[53] Moreover, ACKR1 binds most inflammatory chemokines and regulates their activity via transcytosis across the endothelial barrier.[54] In mice, ACKR1 is only expressed on venular-endothelial cells, and thus leukocyte adhesion to endothelium is restricted to ACKR1$^+$venules.[31] In summary, the expansion of this TEM-enhancing endothelial cell population in the SG supports the likelihood that they contribute to increased lymphocyte infiltration of the pSS, although further experimental evidence is needed.

B cells are known to play a dominant role in the immunopathogenesis of pSS. Consistent with previous studies,[55,56] we found that the proportion of VPREB3$^+$ memory B cells is decreased in PBMCs and increased in the SG of patients with pSS, potentially due to enhanced migration to target organs. The percentage of naive B cells is reportedly higher in PBMCs of patients with pSS than in healthy individuals,[57,58] which is in line with our results showing an expanded IGHD$^+$ naive B cell subpopulation among PBMCs of patients with pSS. We also observed that BANK1$^+$ and CD83$^+$ B cell subsets increased in the SG of patients with pSS, indicating local expansion of effector B cells. However, in a previous study, B-cell depletion with anti-CD20 monoclonal antibody failed due to a relapse in the process of B-cell reconstitution in patients with pSS, indicating that B cell activation factors persist in peripheral blood.[59] In light of the findings in this study, we propose that increased B cell activation in pSS may initiate in the peripheral blood. Thus, an important direction for future research is the characterization of peripheral factors and biomarkers of B-cell activation in patients with pSS.

PD-1$^+$CXCR5$^-$CD4$^+$ Tph cells were previously shown to promote B cell responses in both rheumatoid arthritis and lupus. In pSS, CXCR5$^-$PD1^{hi}ICOS$^+$ Tph cells are known to be enriched in the SG[60] and facilitate B cell recruitment by producing CXCL13.[61] In addition, IL-21, and ICOS expressed by Tph cells promote B cell maturation and survival as well as plasma cell differentiation.[62] In our study, we found that Tph cells with high expression of *CXCL13, CTLA4, ICOS,* and *PDCD1* are enriched in SG, indicating that they play an active role in local B cell activation rather than in peripheral blood. However, the pathological contribution of other expanded FOXP3$^+$CD4$^+$ T cells (Tregs) in pSS remains ambiguous.[63]

The specific role of fibroblasts in the pathogenesis of pSS is also poorly understood. Our results indicate that, in pSS, fibroblasts interact with other cells by downregulating growth signaling factors and extracellular matrix (ECM) components. ECM proteins and their receptor integrins orchestrate several events in SG development and homeostasis.[17] ECM and growth factors are also critical elements for SG tissue engineering approaches.[64] In other inflammatory diseases, such as rheumatoid arthritis and inflammatory bowel disease (IBD), fibroblasts generally exhibit pro-inflammatory functions.[65,66] Korsunsky et al. performed an integrated analysis of fibroblasts from four chronic inflammatory diseases including pSS and found that CXCL10$^+$CCL19$^+$ immune-interacting fibroblasts were expanded in these diseases.[67] Similar to this finding, we identified the fibroblasts interacting with immune cells in pSS with high expression of *CCL19*, *MIF*, *IL-6,* and *MDK*. These results illustrate a dual role for fibroblasts in disrupting ECM formation while promoting inflammatory progression.

In summary, this study defined the function of major stromal cell populations and disease-associated differences between local SG and peripheral blood immune cell populations to clarify the pathological features of pSS. In conclusion, our study provides a preliminary cellular atlas for the SG in Sjögren's Syndrome, opening new avenues of research for therapeutic development to treat this disease.

Limitations of the study

Several limitations of this study warrant mention. In particular, the small subject cohorts used to generate scRNA-seq data of the SG (pSS, n = 11; Ctrl, n = 5) and PBMC populations (pSS, n = 5; Ctrl, n = 3) limit the statistical power of our analyses. Although advanced integrative analysis of published scRNA-seq data from immune cells of five additional patients with pSS and five additional non-SS control subjects helped to support our conclusions regarding the enrichment of B cells and CD4$^+$ T cells in patients with pSS, further scRNA-seq studies investigating the factors and events in pSS pathogenesis in a larger cohort are needed. In addition, labial gland biopsy samples cannot be ethically

or justifiably collected from healthy human subjects. Thus, non-SS SG samples were obtained from patients under evaluation for pSS based on subjective symptoms of dryness but who ultimately did not meet any other classification criteria for pSS. This approach for assembling a control group has been employed in several other studies of the salivary gland microenvironment in pSS.[68–70] The selection criteria applied to the control group samples in the integrated analysis of immune cell subpopulations from SG and PBMCs exhibit some degree of inconsistency. Subsequent scRNA-seq investigations involving paired samples could potentially offer greater insights into the heterogeneity of immune cell subpopulations between local tissue and peripheral compartments.

STAR★METHODS

Detailed methods are provided in the online version of this paper and include the following:

- KEY RESOURCES TABLE
- RESOURCE AVAILABILITY
  - Lead contact
  - Materials availability
  - Data and code availability
- EXPERIMENTAL MODEL AND STUDY PARTICIPANT DETAILS
  - Participants
- METHOD DETAILS
  - Preparation of single-cell suspensions
  - Cell capture and cDNA synthesis
  - Single cell RNA-Seq library preparation
  - scRNA-seq data preprocessing
  - Integration of different batches in scRNA-seq data and identification of cell clusters
  - Differential expression analysis
  - Gene regulatory network analysis
  - Trajectory inference of transition
  - Label mapping analysis
  - Cell-cell communication analysis by CellChat
  - Immunofluorescence assay
  - Sample preparation and flow cytometric analysis
- QUANTIFICATION AND STATISTICAL ANALYSIS

SUPPLEMENTAL INFORMATION

Supplemental information can be found online at https://doi.org/10.1016/j.isci.2023.107943.

ACKNOWLEDGMENTS

This work was supported by the National Natural Science Foundation of China grants (U21A20365 and 81871271 to X.M.L; 32270978 to C.G.), the Fundamental Research Funds for the Central Universities (WK 9110000148 to X.M.L. We thank the USTC supercomputing center and the School of Life Science Bioinformatics Center for providing computing resources for this project.

AUTHOR CONTRIBUTIONS

X.M.L. conceived the study; X.M.L. and C.G. supervised the study; N.X. performed the experiments and conducted all the sample preparation for next-generation sequencing with help from Z.Z., L.W., Z.T., Y.Z., T.Z., Z.C., and J.Z.; H.X. performed the data analysis with help from P.C., K.L., S. L., and M.F.; G.W. contributed to the data interpretation; J. W. contributed to the revision of the article; X.N., C.G., H.X., and X.M.L. wrote the article with the help of all other authors. All authors edited and proofread the article.

DECLARATION OF INTERESTS

There is no competing interest.

Received: April 27, 2023
Revised: August 13, 2023
Accepted: September 14, 2023
Published: September 16, 2023

REFERENCES

1. Qin, B., Wang, J., Yang, Z., Yang, M., Ma, N., Huang, F., and Zhong, R. (2015). Epidemiology of primary Sjogren's syndrome: a systematic review and meta-analysis. Ann. Rheum. Dis. *74*, 1983–1989. https://doi.org/10.1136/annrheumdis-2014-205375.
2. Ramos-Casals, M., Brito-Zerón, P., Sisó-Almirall, A., and Bosch, X. (2012). Primary Sjogren syndrome. BMJ *344*, e3821. https://doi.org/10.1136/bmj.e3821.
3. Henkin, R.I., and Criswell, L.A. (2018). Primary Sjogren's Syndrome. N. Engl. J. Med. *379*, 97. https://doi.org/10.1056/NEJMc1804598.
4. Fox, R.I., Fox, C.M., Gottenberg, J.E., and Dörner, T. (2021). Treatment of Sjogren's syndrome: current therapy and future directions. Rheumatology *60*, 2066–2074. https://doi.org/10.1093/rheumatology/kez142.
5. Fessler, J., Fasching, P., Raicht, A., Hammerl, S., Weber, J., Lackner, A., Hermann, J., Dejaco, C., Graninger, W.B., Schwinger, W., and Stradner, M.H. (2021). Lymphopenia in primary Sjogren's syndrome is associated with premature aging of naive CD4+T cells. Rheumatology *60*, 588–597. https://doi.org/10.1093/rheumatology/keaa105.
6. Asam, S., Neag, G., Berardicurti, O., Gardner, D., and Barone, F. (2021). The role of stroma and epithelial cells in primary Sjogren's syndrome. Rheumatology *60*, 3503–3512. https://doi.org/10.1093/rheumatology/kez050.
7. Kapsogeorgou, E.K., and Manoussakis, M.N. (2010). Salivary gland epithelial cells (SGEC): carriers of exquisite B7-2 (CD86) costimulatory molecules. J. Autoimmun. *35*, 188–191. https://doi.org/10.1016/j.jaut.2010.06.006.
8. Barone, F., Bombardieri, M., Manzo, A., Blades, M.C., Morgan, P.R., Challacombe, S.J., Valesini, G., and Pitzalis, C. (2005). Association of CXCL13 and CCL21 expression with the progressive organization of lymphoid-like structures in Sjogren's syndrome. Arthritis Rheum. *52*, 1773–1784. https://doi.org/10.1002/art.21062.
9. Moriyama, M., Hayashida, J.N., Toyoshima, T., Ohyama, Y., Shinozaki, S., Tanaka, A., Maehara, T., and Nakamura, S. (2012). Cytokine/chemokine profiles contribute to understanding the pathogenesis and diagnosis of primary Sjogren's syndrome. Clin. Exp. Immunol. *169*, 17–26. https://doi.org/10.1111/j.1365-2249.2012.04587.x.
10. Rivière, E., Pascaud, J., Tchitchek, N., Boudaoud, S., Paoletti, A., Ly, B., Dupré, A., Chen, H., Thai, A., Allaire, N., et al. (2020). Salivary gland epithelial cells from patients with Sjogren's syndrome induce B-lymphocyte survival and activation. Ann. Rheum. Dis. *79*, 1468–1477. https://doi.org/10.1136/annrheumdis-2019-216588.
11. Verstappen, G.M., Pringle, S., Bootsma, H., and Kroese, F.G.M. (2021). Epithelial-immune cell interplay in primary Sjogren syndrome salivary gland pathogenesis. Nat. Rev. Rheumatol. *17*, 333–348. https://doi.org/10.1038/s41584-021-00605-2.
12. Turkcapar, N., Sak, S.D., Saatci, M., Duman, M., and Olmez, U. (2005). Vasculitis and expression of vascular cell adhesion molecule-1, intercellular adhesion molecule-1, and E-selectin in salivary glands of patients with Sjogren's syndrome. J. Rheumatol. *32*, 1063–1070.
13. Amft, N., Curnow, S.J., Scheel-Toellner, D., Devadas, A., Oates, J., Crocker, J., Hamburger, J., Ainsworth, J., Mathews, J., Salmon, M., et al. (2001). Ectopic expression of the B cell-attracting chemokine BCA-1 (CXCL13) on endothelial cells and within lymphoid follicles contributes to the establishment of germinal center-like structures in Sjogren's syndrome. Arthritis Rheum. *44*, 2633–2641. https://doi.org/10.1002/1529-0131(200111)44:11<2633::aid-art443>3.0.co;2-9.
14. Nourshargh, S., and Alon, R. (2014). Leukocyte migration into inflamed tissues. Immunity *41*, 694–707. https://doi.org/10.1016/j.immuni.2014.10.008.
15. Kalluri, R. (2016). The biology and function of fibroblasts in cancer. Nat. Rev. Cancer *16*, 582–598. https://doi.org/10.1038/nrc.2016.73.
16. van Ginkel, M.S., Haacke, E.A., Bootsma, H., Arends, S., van Nimwegen, J.F., Verstappen, G.M., Spijkervet, F.K.L., Vissink, A., van der Vegt, B., and Kroese, F.G.M. (2019). Presence of intraepithelial B-lymphocytes is associated with the formation of lymphoepithelial lesions in salivary glands of primary Sjogren's syndrome patients. Clin. Exp. Rheumatol. *7 (Suppl 118)*, S42–S48.
17. Ríos-Ríos, W.d.J., Sosa-Luis, S.A., and Torres-Aguilar, H. (2020). T Cells Subsets in the Immunopathology and Treatment of Sjogren's Syndrome. Biomolecules *10*, 1539. https://doi.org/10.3390/biom10111539.
18. Hansen, A., Odendahl, M., Reiter, K., Jacobi, A.M., Feist, E., Scholze, J., Burmester, G.R., Lipsky, P.E., and Dörner, T. (2002). Diminished peripheral blood memory B cells and accumulation of memory B cells in the salivary glands of patients with Sjogren's syndrome. Arthritis Rheum. *46*, 2160–2171. https://doi.org/10.1002/art.10445.
19. Bird, A.K., Meednu, N., and Anolik, J.H. (2015). New insights into B cell biology in systemic lupus erythematosus and Sjogren's syndrome. Curr. Opin. Rheumatol. *27*, 461–467. https://doi.org/10.1097/BOR.0000000000000201.
20. Seror, R., Ravaud, P., Bowman, S.J., Baron, G., Tzioufas, A., Theander, E., Gottenberg, J.E., Bootsma, H., Mariette, X., and Vitali, C.; EULAR Sjögren's Task Force (2010). EULAR Sjogren's syndrome disease activity index: development of a consensus systemic disease activity index for primary Sjogren's syndrome. Ann. Rheum. Dis. *69*, 1103–1109. https://doi.org/10.1136/ard.2009.110619.
21. Butler, A., Hoffman, P., Smibert, P., Papalexi, E., and Satija, R. (2018). Integrating single-cell transcriptomic data across different conditions, technologies, and species. Nat. Biotechnol. *36*, 411–420. https://doi.org/10.1038/nbt.4096.
22. Barrera, M.J., Bahamondes, V., Sepúlveda, D., Quest, A.F.G., Castro, I., Cortés, J., Aguilera, S., Urzúa, U., Molina, C., Pérez, P., et al. (2013). Sjogren's syndrome and the epithelial target: a comprehensive review. J. Autoimmun. *42*, 7–18. https://doi.org/10.1016/j.jaut.2013.02.001.
23. Costa-da-Silva, A.C., Aure, M.H., Dodge, J., Martin, D., Dhamala, S., Cho, M., Rose, J.J., Bassim, C.W., Ambatipudi, K., Hakim, F.T., et al. (2022). Salivary ZG16B expression loss follows exocrine gland dysfunction related to oral chronic graft-versus-host disease. iScience *25*, 103592. https://doi.org/10.1016/j.isci.2021.103592.
24. Lai, Z., Yin, H., Cabrera-Pérez, J., Guimaro, M.C., Afione, S., Michael, D.G., Glenton, P., Patel, A., Swaim, W.D., Zheng, C., et al. (2016). Aquaporin gene therapy corrects Sjogren's syndrome phenotype in mice. Proc. Natl. Acad. Sci. USA *113*, 5694–5699. https://doi.org/10.1073/pnas.1601992113.
25. Chivasso, C., Nesverova, V., Järvå, M., Blanchard, A., Rose, K.L., Öberg, F.K., Wang, Z., Martin, M., Lhotellerie, F., Zindy, E., et al. (2021). Unraveling Human AQP5-PIP Molecular Interaction and Effect on AQP5 Salivary Glands Localization in SS Patients. Cells *10*, 2108. https://doi.org/10.3390/cells10082108.
26. Aibar, S., González-Blas, C.B., Moerman, T., Huynh-Thu, V.A., Imrichova, H., Hulselmans, G., Rambow, F., Marine, J.C., Geurts, P., Aerts, J., et al. (2017). SCENIC: single-cell regulatory network inference and clustering. Nat. Methods *14*, 1083–1086. https://doi.org/10.1038/nmeth.4463.
27. Tanaka, J., Ogawa, M., Hojo, H., Kawashima, Y., Mabuchi, Y., Hata, K., Nakamura, S., Yasuhara, R., Takamatsu, K., Irié, T., et al. (2018). Generation of orthotopically functional salivary gland from embryonic stem cells. Nat. Commun. *9*, 4216. https://doi.org/10.1038/s41467-018-06469-7.
28. Wang, Y.F., Dang, H.F., Luo, X., Wang, Q.Q., Gao, C., and Tian, Y.X. (2021). Downregulation of SOX9 suppresses breast cancer cell proliferation and migration by regulating apoptosis and cell cycle arrest. Oncol. Lett. *22*, 517. https://doi.org/10.3892/ol.2021.12778.
29. Krüger-Genge, A., Blocki, A., Franke, R.P., and Jung, F. (2019). Vascular Endothelial Cell Biology: An Update. Int. J. Mol. Sci. *20*, 4411. https://doi.org/10.3390/ijms20184411.
30. Kalucka, J., de Rooij, L.P.M.H., Goveia, J., Rohlenova, K., Dumas, S.J., Meta, E., Conchinha, N.V., Taverna, F., Teuwen, L.A., Veys, K., et al. (2020). Single-Cell Transcriptome Atlas of Murine Endothelial Cells. Cell *180*, 764–779.e20. https://doi.org/10.1016/j.cell.2020.01.015.
31. Thiriot, A., Perdomo, C., Cheng, G., Novitzky-Basso, I., McArdle, S., Kishimoto, J.K., Barreiro, O., Mazo, I., Triboulet, R., Ley, K., et al. (2017). Differential DARC/ACKR1 expression distinguishes venular from non-venular endothelial cells in murine tissues. BMC Biol. *15*, 45. https://doi.org/10.1186/s12915-017-0381-7.
32. Kumar, V., Ramnarayanan, K., Sundar, R., Padmanabhan, N., Srivastava, S., Koiwa, M., Yasuda, T., Koh, V., Huang, K.K., Tay, S.T., et al. (2022). Single-Cell Atlas of Lineage States, Tumor Microenvironment, and Subtype-Specific Expression Programs in Gastric Cancer. Cancer Discov. *12*, 670–691. https://doi.org/10.1158/2159-8290.CD-21-0683.
33. Muller, W.A. (2011). Mechanisms of leukocyte transendothelial migration. Annu. Rev. Pathol. *6*, 323–344. https://doi.org/10.1146/annurev-pathol-011110-130224.
34. Setty, M., Kiseliovas, V., Levine, J., Gayoso, A., Mazutis, L., and Pe'er, D. (2019). Characterization of cell fate probabilities in single-cell data with Palantir. Nat. Biotechnol. *37*, 451–460. https://doi.org/10.1038/s41587-019-0068-4.

35. Goules, A.V., Kapsogeorgou, E.K., and Tzioufas, A.G. (2017). Insight into pathogenesis of Sjogren's syndrome: Dissection on autoimmune infiltrates and epithelial cells. Clin. Immunol. *182*, 30–40. https://doi.org/10.1016/j.clim.2017.03.007.
36. Stuart, T., Butler, A., Hoffman, P., Hafemeister, C., Papalexi, E., Mauck, W.M., 3rd, Hao, Y., Stoeckius, M., Smibert, P., and Satija, R. (2019). Comprehensive Integration of Single-Cell Data. Cell *177*, 1888–1902.e21. https://doi.org/10.1016/j.cell.2019.05.031.
37. Hong, X., Meng, S., Tang, D., Wang, T., Ding, L., Yu, H., Li, H., Liu, D., Dai, Y., and Yang, M. (2020). Single-Cell RNA Sequencing Reveals the Expansion of Cytotoxic CD4(+) T Lymphocytes and a Landscape of Immune Cells in Primary Sjogren's Syndrome. Front. Immunol. *11*, 594658. https://doi.org/10.3389/fimmu.2020.594658.
38. Jin, S., Guerrero-Juarez, C.F., Zhang, L., Chang, I., Ramos, R., Kuan, C.H., Myung, P., Plikus, M.V., and Nie, Q. (2021). Inference and analysis of cell-cell communication using CellChat. Nat. Commun. *12*, 1088. https://doi.org/10.1038/s41467-021-21246-9.
39. Wei, K., Nguyen, H.N., and Brenner, M.B. (2021). Fibroblast pathology in inflammatory diseases. J. Clin. Invest. *131*, e149538. https://doi.org/10.1172/JCI149538.
40. Charo, I.F., and Ransohoff, R.M. (2006). The many roles of chemokines and chemokine receptors in inflammation. N. Engl. J. Med. *354*, 610–621. https://doi.org/10.1056/NEJMra052723.
41. Calandra, T., and Roger, T. (2003). Macrophage migration inhibitory factor: a regulator of innate immunity. Nat. Rev. Immunol. *3*, 791–800. https://doi.org/10.1038/nri1200.
42. Maruyama, K., Muramatsu, H., Ishiguro, N., and Muramatsu, T. (2004). Midkine, a heparin-binding growth factor, is fundamentally involved in the pathogenesis of rheumatoid arthritis. Arthritis Rheum. *50*, 1420–1429. https://doi.org/10.1002/art.20175.
43. Witas, R., Gupta, S., and Nguyen, C.Q. (2020). Contributions of Major Cell Populations to Sjogren's Syndrome. J. Clin. Med. *9*, 3057. https://doi.org/10.3390/jcm9093057.
44. Hou, X., Hong, X., Ou, M., Meng, S., Wang, T., Liao, S., He, J., Yu, H., Liu, L., Yin, L., et al. (2022). Analysis of Gene Expression and TCR/B Cell Receptor Profiling of Immune Cells in Primary Sjogren's Syndrome by Single-Cell Sequencing. J. Immunol. *209*, 238–249. https://doi.org/10.4049/jimmunol.2100803.
45. Ninche, N., Kwak, M., and Ghazizadeh, S. (2020). Diverse Epithelial Cell Populations Contribute to the Regeneration of Secretory Units in Injured Salivary Glands. Development *147*, dev192807. https://doi.org/10.1242/dev.192807.
46. Tata, A., Kobayashi, Y., Chow, R.D., Tran, J., Desai, A., Massri, A.J., McCord, T.J., Gunn, M.D., and Tata, P.R. (2018). Myoepithelial Cells of Submucosal Glands Can Function as Reserve Stem Cells to Regenerate Airways after Injury. Cell Stem Cell *22*, 668–683.e6. https://doi.org/10.1016/j.stem.2018.03.018.
47. Xu, X., Xiong, G., Zhang, M., Xie, J., Chen, S., Li, K., Li, J., Bao, Y., Wang, C., and Chen, D. (2022). Sox9(+) cells are required for salivary gland regeneration after radiation damage via the Wnt/beta-catenin pathway. J Genet Genomics *49*, 230–239. https://doi.org/10.1016/j.jgg.2021.09.008.
48. Elmentaite, R., Domínguez Conde, C., Yang, L., and Teichmann, S.A. (2022). Single-cell atlases: shared and tissue-specific cell types across human organs. Nat. Rev. Genet. *23*, 395–410. https://doi.org/10.1038/s41576-022-00449-w.
49. Domenici, G., Aurrekoetxea-Rodríguez, I., Simões, B.M., Rábano, M., Lee, S.Y., Millán, J.S., Comaills, V., Oliemuller, E., López-Ruiz, J.A., Zabalza, I., et al. (2019). A Sox2-Sox9 signalling axis maintains human breast luminal progenitor and breast cancer stem cells. Oncogene *38*, 3151–3169. https://doi.org/10.1038/s41388-018-0656-7.
50. Jana, S., Madhu Krishna, B., Singhal, J., Horne, D., Awasthi, S., Salgia, R., and Singhal, S.S. (2020). SOX9: The master regulator of cell fate in breast cancer. Biochem. Pharmacol. *174*, 113789. https://doi.org/10.1016/j.bcp.2019.113789.
51. Ivetic, A., Hoskins Green, H.L., and Hart, S.J. (2019). L-selectin: A Major Regulator of Leukocyte Adhesion, Migration and Signaling. Front. Immunol. *10*, 1068. https://doi.org/10.3389/fimmu.2019.01068.
52. Carman, C.V., and Springer, T.A. (2004). A transmigratory cup in leukocyte diapedesis both through individual vascular endothelial cells and between them. J. Cell Biol. *167*, 377–388. https://doi.org/10.1083/jcb.200404129.
53. Shulman, Z., Shinder, V., Klein, E., Grabovsky, V., Yeger, O., Geron, E., Montresor, A., Bolomini-Vittori, M., Feigelson, S.W., Kirchhausen, T., et al. (2009). Lymphocyte crawling and transendothelial migration require chemokine triggering of high-affinity LFA-1 integrin. Immunity *30*, 384–396. https://doi.org/10.1016/j.immuni.2008.12.020.
54. Pruenster, M., Mudde, L., Bombosi, P., Dimitrova, S., Zsak, M., Middleton, J., Richmond, A., Graham, G.J., Segerer, S., Nibbs, R.J.B., and Rot, A. (2009). The Duffy antigen receptor for chemokines transports chemokines and supports their promigratory activity. Nat. Immunol. *10*, 101–108. https://doi.org/10.1038/ni.1675.
55. Roberts, M.E.P., Kaminski, D., Jenks, S.A., Maguire, C., Ching, K., Burbelo, P.D., Iadarola, M.J., Rosenberg, A., Coca, A., Anolik, J., and Sanz, I. (2014). Primary Sjogren's Syndrome Is Characterized by Distinct Phenotypic and Transcriptional Profiles of IgD plus Unswitched Memory B Cells. Arthritis Rheumatol. *66*, 2558–2569. https://doi.org/10.1002/art.38734.
56. Hansen, A., Gosemann, M., Pruss, A., Reiter, K., Ruzickova, S., Lipsky, P.E., and Dörner, T. (2004). Abnormalities in peripheral B cell memory of patients with primary Sjogren's syndrome. Arthritis Rheum. *50*, 1897–1908. https://doi.org/10.1002/art.20276.
57. Feng, R., Zhao, J., Sun, F., Miao, M., Sun, X., He, J., and Li, Z. (2022). Comparison of the deep immune profiling of B cell subsets between healthy adults and Sjogren's syndrome. Ann. Med. *54*, 472–483. https://doi.org/10.1080/07853890.2022.2031272.
58. Szabó, K., Jámbor, I., Szántó, A., Horváth, I.F., Tarr, T., Nakken, B., Szodoray, P., and Papp, G. (2021). The Imbalance of Circulating Follicular T Helper Cell Subsets in Primary Sjogren's Syndrome Associates With Serological Alterations and Abnormal B-Cell Distribution. Front. Immunol. *12*, 639975. https://doi.org/10.3389/fimmu.2021.639975.
59. Wang, B., Chen, S., Li, Y., Xuan, J., Liu, Y., and Shi, G. (2021). Targeted Therapy for Primary Sjogren's Syndrome: Where are We Now? BioDrugs *35*, 593–610. https://doi.org/10.1007/s40259-021-00505-7.
60. Pontarini, E., Murray-Brown, W.J., Croia, C., Lucchesi, D., Conway, J., Rivellese, F., Fossati-Jimack, L., Astorri, E., Prediletto, E., Corsiero, E., et al. (2020). Unique expansion of IL-21+ Tfh and Tph cells under control of ICOS identifies Sjogren's syndrome with ectopic germinal centres and MALT lymphoma. Ann. Rheum. Dis. *79*, 1588–1599. https://doi.org/10.1136/annrheumdis-2020-217646.
61. Chen, W., Yang, F., and Lin, J. (2022). Tph Cells Expanded in Primary Sjogren's Syndrome. Front. Med. *9*, 900349. https://doi.org/10.3389/fmed.2022.900349.
62. Rao, D.A. (2018). T Cells That Help B Cells in Chronically Inflamed Tissues. Front. Immunol. *9*, 1924. https://doi.org/10.3389/fimmu.2018.01924.
63. Alunno, A., Carubbi, F., Bistoni, O., Caterbi, S., Bartoloni, E., Mirabelli, G., Cannarile, F., Cipriani, P., Giacomelli, R., and Gerli, R. (2015). T Regulatory and T Helper 17 Cells in Primary Sjogren's Syndrome: Facts and Perspectives. Mediators Inflamm. *2015*, 243723. https://doi.org/10.1155/2015/243723.
64. Piraino, L.R., Benoit, D.S.W., and DeLouise, L.A. (2021). Salivary Gland Tissue Engineering Approaches: State of the Art and Future Directions. Cells *10*, 1723. https://doi.org/10.3390/cells10071723.
65. Kinchen, J., Chen, H.H., Parikh, K., Antanaviciute, A., Jagielowicz, M., Fawkner-Corbett, D., Ashley, N., Cubitt, L., Mellado-Gomez, E., Attar, M., et al. (2018). Structural Remodeling of the Human Colonic Mesenchyme in Inflammatory Bowel Disease. Cell *175*, 372–386.e17. https://doi.org/10.1016/j.cell.2018.08.067.
66. Chibly, A.M., Aure, M.H., Patel, V.N., and Hoffman, M.P. (2022). Salivary gland function, development, and regeneration. Physiol. Rev. *102*, 1495–1552. https://doi.org/10.1152/physrev.00015.2021.
67. Korsunsky, I., Wei, K., Pohin, M., Kim, E.Y., Barone, F., Major, T., Taylor, E., Ravindran, R., Kemble, S., Watts, G.F.M., et al. (2022). Cross-tissue, single-cell stromal atlas identifies shared pathological fibroblast phenotypes in four chronic inflammatory diseases. Med (N Y) *3*, 481–518.e14. https://doi.org/10.1016/j.medj.2022.05.002.
68. Chen, X., Jiang, S., Zhou, Z., Xu, X., Ying, S., Du, L., Qiu, K., Xu, Y., Wu, J., and Wang, X. (2021). Increased expression of interleukin-21-inducible genes in minor salivary glands are associated with primary Sjogren's syndrome disease characteristics. Rheumatology *60*, 2979–2989. https://doi.org/10.1093/rheumatology/keaa695.
69. Oyelakin, A., Horeth, E., Song, E.A.C., Min, S., Che, M., Marzullo, B., Lessard, C.J., Rasmussen, A., Radfar, L., Scofield, R.H., et al. (2020). Transcriptomic and Network Analysis of Minor Salivary Glands of Patients With Primary Sjogren's Syndrome. Front. Immunol. *11*, 606268. https://doi.org/10.3389/fimmu.2020.606268.
70. Wang, X., Pang, K., Wang, J., Zhang, B., Liu, Z., Lu, S., Xu, X., Zhu, L., Zhou, Z., Niu, M., et al. (2022). Microbiota dysbiosis in primary Sjogren's syndrome and the ameliorative

effect of hydroxychloroquine. Cell Rep. *40*, 111352. https://doi.org/10.1016/j.celrep.2022.111352.

71. Zhou, Y., Zhou, B., Pache, L., Chang, M., Khodabakhshi, A.H., Tanaseichuk, O., Benner, C., and Chanda, S.K. (2019). Metascape provides a biologist-oriented resource for the analysis of systems-level datasets. Nat. Commun. *10*, 1523. https://doi.org/10.1038/s41467-019-09234-6.
72. Moon, K.R., van Dijk, D., Wang, Z., Gigante, S., Burkhardt, D.B., Chen, W.S., Yim, K., Elzen, A.V.D., Hirn, M.J., Coifman, R.R., et al. (2019). Visualizing structure and transitions in high-dimensional biological data. Nat. Biotechnol. *37*, 1482–1492. https://doi.org/10.1038/s41587-019-0336-3.
73. Shiboski, C.H., Shiboski, S.C., Seror, R., Criswell, L.A., Labetoulle, M., Lietman, T.M., Rasmussen, A., Scofield, H., Vitali, C., Bowman, S.J., et al. (2017). 2016 American College of Rheumatology/European League Against Rheumatism Classification Criteria for Primary Sjögren's Syndrome: A Consensus and Data-Driven Methodology Involving Three International Patient Cohorts. Arthritis Rheumatol. *69*, 35–45. https://doi.org/10.1002/art.39859.
74. Fleming, S.J., Chaffin, M.D., Arduini, A., Akkad, A.-D., Banks, E., Marioni, J.C., Philippakis, A.A., Ellinor, P.T., and Babadi, M. (2022). Unsupervised removal of systematic background noise from droplet-based single-cell experiments using <kbd>CellBender</kbd>. Preprint at bioRxiv. https://doi.org/10.1101/791699.
75. Germain, P.L., Lun, A., Garcia Meixide, C., Macnair, W., and Robinson, M.D. (2021). Doublet identification in single-cell sequencing data using scDblFinder. F1000Res. *10*, 979. https://doi.org/10.12688/f1000research.73600.2.

STAR★METHODS

KEY RESOURCES TABLE

REAGENT or RESOURCE	SOURCE	IDENTIFIER
Antibodies		
FITC anti-human CD19(clone HIB19)	BioLegend	Cat# 302206; RRID: AB_314236
PE/Cyanine7 anti-human CD27(clone O323)	BioLegend	Cat#302837; RRID: AB_2561918
Brilliant Violet 421™ anti-human IgD (clone IA6-2)	BioLegend	Cat#348225; RRID: AB_2561618
APC anti-human CD29 (ITGB1) (clone TS2/16)	BioLegend	Cat#303007; RRID: AB_314323
PE anti-human MRP-14 (S100A9) (clone MRP 1H9)	BioLegend	Cat#350705; RRID: AB_2564007
FITC anti-human CD4(clone RPA-T4)	BioLegend	Cat#300506; RRID: AB_314074
APC anti-human CD314 (KLRK1) (clone 1D11)	BioLegend	Cat#320807; RRID: AB_492963
PE anti-human FOXP3(PCH101)	eBioscience	Cat#12-4776-42; RRID: AB_1518782
Rabbit Polyclonal anti-smooth muscle actin (α-SMA)	Proteintech	Cat# 14395-1-AP; RRID: AB_2223009
Rabbit Monoclonal anti-SOX9	Abcam	Cat# ab185966; RRID: AB_2728660
Mouse Anti-Human CD31 (PECAM-1) Monoclonal Antibody	Cell Signaling Technology	Cat#3528S; RRID: AB_2160882
Rabbit polyclonal to DARC (ACKR1)	Abcam	Cat#ab124648; RRID: AB_10973364
Biological samples		
Patient samples (blood and MSG biopsies)	The First Affiliated Hospital of USTC	N/A
Chemicals, peptides, and recombinant proteins		
MACS Tissue Storage Solution	Miltenyi	Cat#130-100-008
collagenase II	Sigma	Cat#C6885
CaCl2	ALADDIN	Cat#C290948
DNAse I	Sigma	Cat# D5025
dispase	Sigma	Cat# P3417-10G
trypan blue	Sigma	Cat#T6146
red blood cell lysis buffer	Solarbio	Cat#R1010
xylene	Sinopharm Chemical Reagent Co., Ltd	Cat# 10023418
ethanol	Sinopharm Chemical Reagent Co., Ltd	Cat# 100092683
10% neutral formalin	Solarbio	Cat#G2161
sodium citrate	Solarbio	Cat#C1031
Human Lymphocyte Separation Medium	TBD	Cat#LTS1077-1
Intracellular Fixation & Permeabilization Buffer Set	eBioscience	Cat#88-8824-00
Critical commercial assays		
Single Cell 3′ Library and Gel Bead Kit V3	10x Genomics	Cat#1000075
Chromium Single Cell B Chip Kit	10x Genomics	Cat#1000074
Four-color multi-label immunofluorescence kit	Absin	Cat#abs50012
Deposited data		
scRNA-seq of pSS patients and controls	This paper	GSA record HRA003613
scRNA-seq data	https://www.frontiersin.org/articles/10.3389/fimmu.2020.594658/full	GEO: GSE157278

(*Continued on next page*)

Continued

REAGENT or RESOURCE	SOURCE	IDENTIFIER
RNA sequencing data of SOX9-knockdown in breast cancer cell	https://www.spandidos-publications.com/10.3892/ol.2021.12778	GEO: PRJNA721654
Software and algorithms		
CytExpert software 2.4	Beckman Coulter	https://www.beckman.fr/flow-cytometry/instruments/cytoflex/software; RRID:SCR_017217
Cell Ranger Software Suite (v.3.0.0)	10X Genomics	https://support.10xgenomics.com/single-cell-gene-expression/software/pipelines/latest/what-is-cell-ranger; RRID:SCR_017344
Seurat R Package (v.3)	Stuart et al.[1]	https://satijalab.org/seurat/get_started.html; RRID:SCR_016341
Metascape	Zhou et al.[71]	http://metascape.org/gp/index.html#/main/step1; RRID:SCR_016620
SCENIC	Aibar et al.[26]	https://github.com/aertslab/SCENIC; RRID:SCR_017247
PHATE	Moon et al.[72]	NA
Palantir	Setty et al.[34]	NA
CellChat (version 1.5.0)	Jin et al.[38]	https://github.com/sqjin/CellChat; RRID:SCR_021946
GraphPad Prism 9	GraphPad	http://www.graphpad.com/; RRID:SCR_002798
biorender	SciCrunch Registry	https://www.biorender.com/; RRID:SCR_018361
Code in this study	This paper	https://github.com/Bink98/pSS_scRNAseq_analysis

RESOURCE AVAILABILITY

Lead contact

Further information and requests for resources and data should be directed to and will be fulfilled by the lead contact, Xiaomei Li (lixiaomei@ustc.edu.cn).

Materials availability

This study did not generate new unique reagents.

Data and code availability

- Raw data for single-cell RNA-seq samples have been deposited in the Genome Sequence Archive (GSA) in the National Genomics Data Center under accession number HRA003613. This paper analyzes existing, publicly available data. These accession numbers for the datasets are listed in the key resources table.
- The code for all analyses is available at Github: https://github.com/Bink98/pSS_scRNAseq_analysis.
- Any additional information required to reanalyze the data reported in this paper is available from the lead contact upon request.

EXPERIMENTAL MODEL AND STUDY PARTICIPANT DETAILS

Participants

This study was approved by the Ethics Committee of the First Affiliated Hospital of University of Science and Technology of China (No. 2021-KY-247). Each participant provided written informed consent. Eleven patients with pSS from the department of Rheumatology and Immunology, the First Affiliated Hospital of University of Science and Technology of China, were recruited for this study. All pSS patients fulfilled the diagnosis of pSS according to the classification criteria established by the 2016 American College of Rheumatology (ACR)/European League against Rheumatism (EULAR).[73] Five non-SS subjects who had experienced subjective symptoms of dryness but did not meet any of the classification criteria for pSS were also included. All 11 pSS and 5 non-SS participants agreed to undergo a biopsy of the labial salivary

gland under local anesthesia following standard methods. No clinical interventions were initiated before biopsies were taken. Subjects with other autoimmune diseases, acute infections, immunodeficiency or malignant tumors were not enrolled in this study. In addition, we collected another cohort for blood single-cell RNA sequencing, including an additional 5 pSS patients who fulfilled the same selection criteria and 3 healthy individuals. Peripheral venous blood samples (5 mL) were obtained. Participant demographics, classification criteria, clinical manifestations, and EULAR Sjögren's syndrome disease activity index (ESSDAI) scores are summarized in Table S1.

METHOD DETAILS

Preparation of single-cell suspensions

Following resection in the operating room, part of the fresh labial salivary gland lesions was stored in MACS Tissue Storage Solution after rinsing with 1×DPBS and transported rapidly to the research facility. Additional glands from these patients were submitted for histopathological assessment, including focus scoring. On arrival, the specimens were washed with Hanks Balanced Salt Solution (HBSS) three times and minced on ice into 1 mm smaller pieces. Then, the tissue pieces were digested with 2 mL of tissue dissociation solution containing collagenase II, $CaCl_2$, DNAse I, dispase and 2% FBS at 37°C for 90 min, with manual blowing every 15 min. After digestion, the samples were filtered through 70-μm nylon mesh (Thermo Fisher Scientific) and centrifuged at 500 × g for 10 min. Subsequently, the supernatants were discarded, and the cell pellets were suspended in 1 mL phosphate-buffered saline (PBS. To lyse red blood cells, 2 mL of red blood cell lysis buffer was added, and the cells were incubated at 25°C for 5 min. After washing twice with PBS, the cell pellets were resuspended in PBS. Next, 10 μL of this cell suspension was mixed with 10 μL of trypan blue, and an automated cell counter was used to determine the concentration of live cells. Suspensions with greater than 85% viability were used for subsequent sequencing.

Peripheral blood mononuclear cells (PBMCs) were isolated from heparinized venous blood of pSS patients or controls using a Ficoll-Hypaque density solution according to standard density gradient centrifugation methods. Briefly, blood was mixed with an equal volume of PBS, and then the diluted sample was added to an equal volume of peripheral blood mononuclear lymphocyte separation solution. Cells were centrifuged at 500 × g for 30 min at 4°C. The mononuclear cell layer between the plasma layer and the separation layer was carefully aspirated, 5–10 mL PBS was added to wash the cells 1–2 times. To lyse red blood cells, 2 mL of red blood cell lysis buffer was added, and the cells were incubated at 25°C for 5 min, and the cells were counted. The cells in the middle layer were then washed once with PBS and resuspended in PBS for use.

Cell capture and cDNA synthesis

Using the Single Cell 3′ Library and Gel Bead Kit V3 (10x Genomics, 1000075) and Chromium Single Cell B Chip Kit (10x Genomics, 1000074), the cell suspension (300–600 living cells per microliter determined by Count Star) was loaded onto the Chromium Single Cell Controller (10x Genomics) to generate single-cell gel beads in the emulsion according to the manufacturer's protocol. In short, single cells were suspended in PBS containing 0.04% BSA. Approximately 6,000 cells were added to each channel, and the target cell that was recovered was estimated to be approximately 3,000 cells. Captured cells were lysed, and the released RNA was barcoded through reverse transcription in individual GEMs. Reverse transcription was performed on an S1000TM Touch Thermal Cycler (Bio-Rad) at 53°C for 45 min, followed by 85°C for 5 min, and hold at 4°C. The cDNA was generated and then amplified, and quality was assessed using an Agilent 4200.

Single cell RNA-Seq library preparation

According to the manufacturer's instructions, single-cell RNA-seq libraries were constructed using the Single Cell 3′ Library and Gel Bead Kit V3. The libraries were finally sequenced using an Illumina Novaseq6000 sequencer with a sequencing depth of at least 100,000 reads per cell with a paired-end 150 bp (PE150) reading strategy.

scRNA-seq data preprocessing

Droplet-based raw data were processed using Cell Ranger (Version 3.0.0) against the GRCh38 human reference genome with default parameters. We first remove the background in the SG samples by using CellBender with FPR = 0.01.[74] Then, based on the background-removed raw count matrix, we removed potential doublets using scDblFinder[75] with default parameters after removing empty cells (fewer than 100 detected genes and fewer than 200 UMIs). We also filtered out cells with fewer than 500 detected genes and higher than 25% mitochondrial UMIs for SG data and fewer than 800 detected genes and higher than 15% mitochondrial UMIs for PBMC data.

Integration of different batches in scRNA-seq data and identification of cell clusters

Data from each batch were normalized separately using the NormalizeData function and scaled with the ScaleData function implemented in the Seurat pipeline.[36] For SG batches, we obtained the top 3000 most variable genes of each batch. Then, we retained the top 3000 most variable genes for integrated analysis of SG data. We ran Harmony with PCA embeddings (30 PCs) as input, with default parameters to eliminate the batch effects among sixteen batches (11 pSS samples, 5 non-SS samples). Subsequently, Harmony embeddings were applied to identify the clusters using the FindCluster function in Seurat with resolution = 2. We removed one cluster without obvious marker genes in downstream analysis. To integrate the immune cells of SGs and PBMCs, we used the canonical correlation analysis (CCA) method implemented in Seurat. Then, we obtained PCA embedding with an integrated expression matrix. We then used the same clustering algorithm as that used in SG to cluster the cells with resolution 2 to generate distinct cell-type clusters.

Differential expression analysis

To identify the DEGs in different clusters or disease/control states, we performed differential expression analysis using the built-in function "scanpy.tl.rank_genes_groups" in Scanpy using the Wilcoxon rank-sum test. Then, we retained the DEGs with multiple thresholds (fold change $\geq$0.5, adjusted p value $\leq$0.01, and fraction of cells expressing the genes in both clusters >10%) to identify marker genes expressed in each cell subset and differentially expressed genes between non-SS and pSS. We then performed gene set enrichment analysis using Metascape.[71] In Figure 1E, we calculated the DEG numbers in different cell types between non-SS and pSS samples by combining all subcluster DEGs.

Gene regulatory network analysis

To explore the regulon activity in SG cells, we used the pySCENIC[26] package to predict activated TFs in all SG cells. We performed gene regulatory network inference by following the tutorial https://github.com/aertslab/SCENICprotocol/blob/master/notebooks/PBMC10k_SCENIC-protocol-CLI.ipynb. We first built a co-expression network to target TFs with the package GENIE3. DNA motif analysis was performed with cisTarget, after which each cell was scored by AUCell. In Figure 2F, we ranked the TFs by the proportion of TF target genes predicted by SCENIC overlapped with a gene set (e.g., epithelial cell differentiation) overall target genes.

Trajectory inference of transition

Dimensionality reduction was performed based on Harmony embeddings by using PHATE, a dimensionality-reduction method that is capable of capturing both local and global structures.[72] We conducted trajectory inference using Palantir[34] with default parameters. We determined the trends of gene expression along pseudotime by Palantir. As implemented in Palantir, clustering of the gene expression trends was generated based on the Phenograph algorithm.

Label mapping analysis

We reanalyzed another recently published single-cell transcriptome of PBMCs from pSS patients. We downloaded the raw expression matrix from GEO (GSE157278). We used the FindTransferAnchors and FindTransterData functions in Seurat[36] to project the cell annotations in this study to the unannotated data based on the PCA embeddings.

Cell-cell communication analysis by CellChat

CellChat (version 1.5.0)[38] enables the comparison framework by systematically detecting cell-cell communication across biological conditions. Here, we performed cell-cell communication prediction analysis by following the tutorial https://htmlpreview.github.io/?https://github.com/sqjin/CellChat/blob/master/tutorial/Comparison_analysis_of_multiple_datasets.html. To identify the interactions between which cell subpopulations showed significant changes, we first computed and visualized the differential interaction strength among different cell subpopulations by the netVisual_diffInteraction and netVisual_heatmap functions with default parameters. Additionally, we compared the outgoing (as sources/ligand) and incoming (as receiver/receptor) interaction strengths between the pSS patients and non-SS controls by the netAnalysis_signalingRole_scatter function. Furthermore, we identified the specific signaling changes of the fibroblast cells between the pSS patients and non-SS controls by netAnalysis_signalingChanges_scatter function. To identify dysfunctional signaling, including the upregulated and downregulated ligand-receptor pairs, we performed differential expression analysis between the pSS patients and non-SS controls for each cell subpopulation by the identifyOverExpressedGenes function with parameters (only.pos = FALSE, thresh.pc = 0.1, thresh.fc = 0.1, thresh.p = 1). To obtain the significantly upregulated (thresh = 0.01, ligand.logFC = 0.1, receptor.logFC = 0.1) and downregulated (thresh = 0.01, ligand.logFC = −0.1, receptor.logFC = −0.1) signaling in the pSS patients, we selected the interactions based on the fold change of ligands in the sender cells and receptors in the receiver cells.

Immunofluorescence assay

Formalin-fixed paraffin-embedded labial salivary gland (LSG) tissue sections from pSS patients and non-SS controls were deparaffinized in xylene and rehydrated with graded ethanol (100%, 95%, 70%, and 50%). Tissue sections were washed and then infiltrated in 10% neutral formalin for 10 min. Next, the antigen was repaired, and the slides were placed into boiling sodium citrate and heated for 4 min. After cooling to room temperature, tissue slices were blocked in goat serum at 37°C for 30 min to prevent background staining. Subsequently, tissue sections were incubated with the relevant primary antibody at 4°C overnight. After a 1 h incubation with the relevant secondary antibody (1:100) at room temperature, the slides were incubated in the amplification diluent containing a tyramide-conjugated fluorophore for 10 min. Prior to the next primary antibody incubation, the slides were heated in 10 mm citric acid (pH 6.0) for 10 min at 95°C to strip the antibodies of the previous staining round. The protocol was repeated from the blocking step until a total of two markers were co-stained. After the last round of staining, the slides were washed, incubated with 0.5 g/mL 4′,6 diamidine-2-phenylindole (DAPI) for 5 min. The following set of markers was analyzed for each sample (indicated in the order of staining): anti-human SOX9 antibody (Abcam, ab185966), anti-human ACKR1 antibody (Abcam, ab124648), anti-human α-SMA antibody (Proteintech, 14395-1-AP), and anti-human CD31 antibody (Cell Signaling Technologies, CST, 3528S). Images were obtained using a Zeiss Spot inverted fluorescence microscope (Carl Zeiss, Gottingen, Germany).

Sample preparation and flow cytometric analysis

20 pSS patients who fulfilled the same selection criteria and 10 healthy individuals were involved for the flow cytometric analysis. 5 mL blood was collected from pSS patients and control subject in vacutainer tubes containing ethylenediaminetetraacetic acid (EDTA). PBMCs were isolated from peripheral blood by Ficoll density-gradient centrifugation. PBMCs then were labeled with fluorescent antibodies fluorochrome-conjugated antibodies against the markers described in Figures S7 and S8 accordance to the operating instructions. Intracellular proteins were also labeled using the permeabilization kit. The percentages of B and $CD4^{+}$T cell subsets were determined by flow assay using CytoFLEX S flow cytometry instrument. CytExpert software was used for analysis.

QUANTIFICATION AND STATISTICAL ANALYSIS

The statistical tests used here are indicated in the relevant figure legends. Data are presented as the mean ± standard deviation (SD) or median (interquartile range, IQR). We used the Wilcoxon rank-sum test to assess differences in the proportions of cell types in non-SS controls versus pSS patients. Gene expression and gene set expression between non-SS controls versus pSS patients were analyzed using the Wilcoxon rank-sum test. To identify marker genes expressed in each subset and the differentially expressed genes between the Wilcoxon rank-sum test, we used the Wilcoxon rank-sum tests implemented in Scanpy. Flow cytometry data were analyzed using CytExpert software 2.4 (Beckman Coulter). Mann-Whitney U test was used to determine the significance between groups for flow cytometric data. Statistical analyses and approximations were performed with GraphPad Prism v9 software (GraphPad). A p value of less than 0.05 was considered statistically significant, *$p < 0.05$, **$p < 0.01$, ***$p < 0.001$, ****$p < 0.0001$.